Green's function representations for Marchenko imaging without up/down decomposition

Kees Wapenaar [1], Roel Snieder,[2] Sjoerd de Ridder [3] and Evert Slob [1]

[1]*Department of Geoscience and Engineering, Delft University of Technology, P.O. Box 5048, 2600 GA Delft, the Netherlands. E-mail:*
c.p.a.wapenaar@tudelft.nl
[2]*Center for Wave Phenomena, Colorado School of Mines, Golden, CO 80401, USA*
[3]*School of Earth and Environment, University of Leeds, Leeds, LS29JT, United Kingdom*

SUMMARY
Marchenko methods are based on integral representations which express Green's functions for virtual sources and/or receivers in the subsurface in terms of the reflection response at the surface. An underlying assumption is that inside the medium the wave field can be decomposed into downgoing and upgoing waves and that evanescent waves can be neglected. We present a new derivation of Green's function representations which circumvents these assumptions, both for the acoustic and the elastodynamic situation. These representations form the basis for research into new Marchenko methods which have the potential to handle refracted and evanescent waves and to more accurately image steeply dipping reflectors.

Key words: Controlled source seismology; Seismic interferometry; Wave scattering and diffraction.

1 INTRODUCTION

Marchenko redatuming, imaging, monitoring and multiple elimination are all derived from integral representations which express Green's functions for virtual sources or receivers in the subsurface in terms of the reflection response at the surface (Ravasi *et al.* 2016; Jia *et al.* 2018; Staring *et al.* 2018; Brackenhoff *et al.* 2019; Lomas & Curtis 2019; Mildner *et al.* 2019; Elison *et al.* 2020; Reinicke *et al.* 2020; Zhang & Slob 2020). These representations, in turn, are derived from reciprocity theorems for one-way wave fields (Slob *et al.* 2014; Wapenaar *et al.* 2014), building on ideas presented by Broggini & Snieder (2012). Marchenko methods deal with internal multiples in a data-driven way and have the potential to solve large-scale 3-D imaging and multiple elimination problems (Pereira *et al.* 2019; Staring & Wapenaar 2020; Ravasi & Vasconcelos 2021). Of course Marchenko methods have also limitations. One of the limitations is caused by the fact that the one-way reciprocity theorems require that the wave field in the subsurface region of interest can be decomposed into downgoing and upgoing fields. Moreover, one of these reciprocity theorems (the correlation-type theorem) is based on the assumption that evanescent waves can be neglected. These assumptions complicate the imaging of steep flanks and exclude a proper treatment of refracted waves and evanescent waves tunnelling through high velocity layers.

To address some of the limitations, Kiraz *et al.* (2021) propose a Marchenko method without decomposition inside the medium, assuming the input data are acquired on a closed boundary. On the other hand, for reflection data on a single horizontal boundary, a first step has been made towards a Marchenko method that deals with evanescent waves (Wapenaar 2020). This method is restricted to horizontally layered media and uses wave field decomposition inside the medium.

In this paper, we derive more general Green's function representations which do not rely on wave field decomposition in the subsurface and which hold for an arbitrarily inhomogeneous medium below a single horizontal acquisition boundary. These representations form a starting point for new research on Marchenko methods which circumvent several of the present limitations. Diekmann & Vasconcelos (2021) independently investigate the same problem, but without specifying a focusing condition for their focusing function *f* and requiring a time-symmetric source function for *f*. Our derivation follows a different approach, using an explicit focusing condition and requiring no source function for our focusing function *f*. Moreover, we derive several forms of Green's function representations, including one for the homogeneous Green's function between a virtual source and a virtual receiver in the subsurface. We also derive elastodynamic versions of these representations.

This paper is restricted to the derivation of the Green's function representations; a discussion of their application in new Marchenko methods is beyond the scope of this paper.
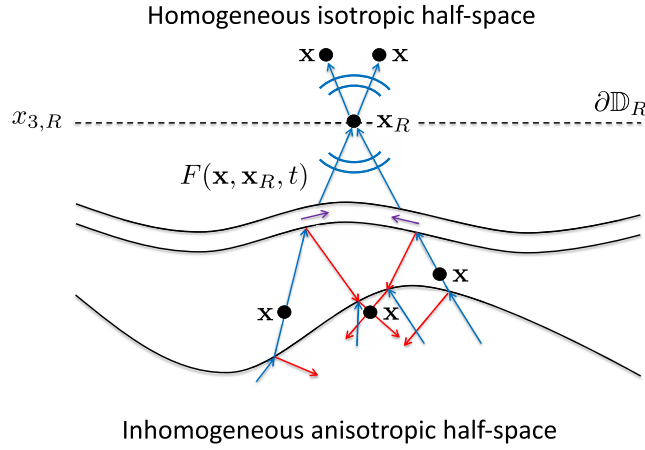
Homogeneous isotropic half-space

Inhomogeneous anisotropic half-space

Figure 1. Illustration of the focusing function $F(\mathbf{x}, \mathbf{x}_R, t)$, which focuses at $\mathbf{x}_R$. For $\mathbf{x}$ at and above $\partial\mathbb{D}_R$ it is purely upgoing. For $\mathbf{x}$ in the half-space below $\partial\mathbb{D}_R$ it is a complex wave field. The near-horizontal arrows in the thin layer illustrate tunnelling evanescent waves.

2 ACOUSTIC WAVE FIELD REPRESENTATION

We consider a lossless acoustic medium, consisting of a homogeneous isotropic upper half-space and an arbitrary inhomogeneous anisotropic lower half-space, separated by a horizontal surface $\partial\mathbb{D}_R$. Coordinates in the medium are denoted by $\mathbf{x} = (\mathbf{x}_H, x_3)$, with $\mathbf{x}_H = (x_1, x_2)$ denoting the horizontal coordinates and x_3 the depth coordinate (the positive x_3-axis is pointing downward). The horizontal surface $\partial\mathbb{D}_R$ is defined at $x_3 = x_{3,R}$ (in the next section we choose this as the surface at which seismic acquisition takes place). The medium parameters of the lower half-space $x_3 > x_{3,R}$ are the compressibility $\kappa(\mathbf{x})$ and the mass density tensor $\rho_{jk}(\mathbf{x})$. At the micro scale (much smaller than the wavelength of the acoustic field) the mass density is isotropic. However, small-scale heterogeneities of the isotropic mass density, for example caused by fine-layering, may manifest themselves as effective anisotropy at the scale of the wavelength (Schoenberg & Sen 1983). The mass density tensor is symmetric, that is, $\rho_{jk}(\mathbf{x}) = \rho_{kj}(\mathbf{x})$. The parameters of the upper half-space $x_3 < x_{3,R}$ are the constant compressibility $\kappa = \kappa_0$ and the constant isotropic mass density $\rho_{jk} = \delta_{jk}\rho_0$, where δ_{jk} is the Kronecker delta function. The propagation velocity of the upper half-space is $c_0 = (\kappa_0\rho_0)^{-1/2}$. At $\partial\mathbb{D}_R$ we choose the same constant isotropic medium parameters as in the upper half-space.

The basic equations for acoustic wave propagation are the linearized equation of motion

$$\rho_{jk}\partial_t v_k + \partial_j p = 0 \tag{1}$$

and the linearized deformation equation

$$\kappa\partial_t p + \partial_i v_i = q, \tag{2}$$

respectively. Here $p(\mathbf{x}, t)$ is the space ($\mathbf{x}$) and time (t) dependent acoustic pressure, $v_i(\mathbf{x}, t)$ the particle velocity and $q(\mathbf{x}, t)$ a source in terms of volume-injection rate density. Operator ∂_i stands for differentiation in the x_i-direction. Lower-case subscripts (except t) take on the values 1, 2 and 3, and the summation convention applies to repeated subscripts. Operator ∂_t stands for differentiation with respect to time. We introduce the specific volume tensor $\vartheta_{ij}(\mathbf{x})$ as the inverse of the mass density tensor, with $\vartheta_{ij}\rho_{jk} = \delta_{ik}$. Applying the operator $\partial_i\vartheta_{ij}$ to eq. (1), operator ∂_t to eq. (2), and subtracting the two equations yields the acoustic wave equation

$$\partial_i(\vartheta_{ij}\partial_j p) - \kappa\partial_t^2 p = -\partial_t q. \tag{3}$$

We introduce a focusing function $F(\mathbf{x}, \mathbf{x}_R, t)$, in which $\mathbf{x}_R = (\mathbf{x}_{H,R}, x_{3,R})$ denotes the position of a focal point at $\partial\mathbb{D}_R$ (Fig. 1). For fixed $\mathbf{x}_R$ and variable $\mathbf{x}$ and t, this focusing function is a solution of wave eq. (3) for the source-free situation, hence, for $q = 0$. We define the focusing condition as

$$F(\mathbf{x}, \mathbf{x}_R, t)|_{x_3=x_{3,R}} = \delta(\mathbf{x}_H - \mathbf{x}_{H,R})\delta(t), \tag{4}$$

and further demand that $F(\mathbf{x}, \mathbf{x}_R, t)$ is purely upgoing at $\partial\mathbb{D}_R$ and in the homogeneous isotropic upper half-space. Note that $F(\mathbf{x}, \mathbf{x}_R, t)$ is similar, but not identical, to the focusing function $f_2(\mathbf{x}, \mathbf{x}_R, t)$ introduced in Wapenaar *et al.* (2014). We come back to this in Section 3.2.

We define the temporal Fourier transform of a space- and time-dependent function $u(\mathbf{x}, t)$ as

$$u(\mathbf{x}, \omega) = \int_{-\infty}^{\infty} u(\mathbf{x}, t)\exp(i\omega t)\mathrm{d}t, \tag{5}$$

where ω is the angular frequency and i the imaginary unit. The integral is taken from $t = -\infty$ to $t = \infty$ to account for non-causal functions, such as the focusing function $F(\mathbf{x}, \mathbf{x}_R, t)$ for which no causality condition is implied (hence, in general it can be non-zero for positive and negative time). With this transform, wave eq. (3) transforms to

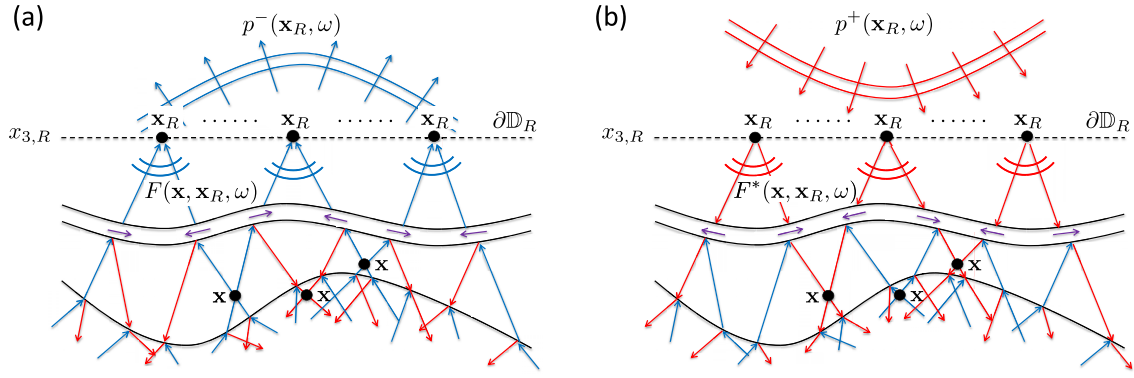$$\mathcal{L}p = i\omega q, \tag{6}$$

Figure 2. Explanation of the first (a) and second (b) integral in eq. (11) in terms of Huygens' principle. The focusing functions $F(\mathbf{x}, \mathbf{x}_R, \omega)$ and $F^*(\mathbf{x}, \mathbf{x}_R, \omega)$ propagate the fields $p^-(\mathbf{x}_R, \omega)$ and $p^+(\mathbf{x}_R, \omega)$ from all $\mathbf{x}_R$ at the surface $\partial\mathbb{D}_R$ to $\mathbf{x}$ in the lower half-space. The superposition of these propagated fields gives the field $p(\mathbf{x}, \omega)$ for any $\mathbf{x}$ in the lower half-space.

with

$$\mathcal{L} = \partial_i \vartheta_{ij} \partial_j + \omega^2 \kappa. \tag{7}$$

The focusing function $F(\mathbf{x}, \mathbf{x}_R, \omega)$ obeys in the frequency domain the wave equation

$$\mathcal{L}F = 0, \tag{8}$$

the focusing condition

$$F(\mathbf{x}, \mathbf{x}_R, \omega)|_{x_3 = x_{3,R}} = \delta(\mathbf{x}_\mathrm{H} - \mathbf{x}_{\mathrm{H},R}), \tag{9}$$

and it is upgoing at and above $\partial\mathbb{D}_R$. We discuss a representation for a wave field $p(\mathbf{x}, \omega)$, which may have sources in the upper half-space above $\partial\mathbb{D}_R$, but which obeys the source-free wave equation $\mathcal{L}p = 0$ for $x_3 \geq x_{3,R}$. In the lower half-space we express $p(\mathbf{x}, \omega)$ as a superposition of mutually independent wave fields that obey the same source-free wave equation as $p(\mathbf{x}, \omega)$ for $x_3 \geq x_{3,R}$. For this purpose, we choose the focusing functions $F(\mathbf{x}, \mathbf{x}_R, \omega)$ and $F^*(\mathbf{x}, \mathbf{x}_R, \omega)$ (the asterisk denotes complex conjugation, which corresponds to time-reversal in the time domain). To be more specific, we express $p(\mathbf{x}, \omega)$ as

$$p(\mathbf{x}, \omega) = \int_{\partial\mathbb{D}_R} F(\mathbf{x}, \mathbf{x}_R, \omega) a(\mathbf{x}_R, \omega) \mathrm{d}\mathbf{x}_R + \int_{\partial\mathbb{D}_R} F^*(\mathbf{x}, \mathbf{x}_R, \omega) b(\mathbf{x}_R, \omega) \mathrm{d}\mathbf{x}_R, \quad \text{for} \quad x_3 \geq x_{3,R}. \tag{10}$$

Here $a(\mathbf{x}_R, \omega)$ and $b(\mathbf{x}_R, \omega)$ are as yet undetermined coefficients, which depend on the position $\mathbf{x}_R$ at $\partial\mathbb{D}_R$. In Appendix A1 we formulate boundary conditions for the acoustic pressure and the vertical component of the particle velocity at $\partial\mathbb{D}_R$, from which we solve $a(\mathbf{x}_R, \omega)$ and $b(\mathbf{x}_R, \omega)$. We thus obtain

$$p(\mathbf{x}, \omega) = \int_{\partial\mathbb{D}_R} F(\mathbf{x}, \mathbf{x}_R, \omega) p^-(\mathbf{x}_R, \omega) \mathrm{d}\mathbf{x}_R + \int_{\partial\mathbb{D}_R} F^*(\mathbf{x}, \mathbf{x}_R, \omega) p^+(\mathbf{x}_R, \omega) \mathrm{d}\mathbf{x}_R, \quad \text{for} \quad x_3 \geq x_{3,R}, \tag{11}$$

where $p^-(\mathbf{x}_R, \omega)$ and $p^+(\mathbf{x}_R, \omega)$ represent the upgoing $(-)$ and downgoing $(+)$ parts, respectively, of $p(\mathbf{x}_R, \omega)$ for $\mathbf{x}_R$ at $\partial\mathbb{D}_R$. These upgoing and downgoing fields are pressure-normalized, meaning that $p^- + p^+ = p$ at and above $\partial\mathbb{D}_R$. Below $\partial\mathbb{D}_R$ we only consider the total (undecomposed) wave field p.

For an intuitive explanation of the right-hand side of eq. (11) we refer to Fig. 2. First we consider the second integral, which is illustrated in Fig. 2(b). The downgoing field $p^+(\mathbf{x}_R, \omega)$ is incident from the homogeneous upper half-space to $\partial\mathbb{D}_R$. The complex conjugate focusing function $F^*(\mathbf{x}, \mathbf{x}_R, \omega)$ propagates this downgoing field from $\mathbf{x}_R$ at $\partial\mathbb{D}_R$ to $\mathbf{x}$ in the lower half-space and the integral superposes the contributions from all $\mathbf{x}_R$ at $\partial\mathbb{D}_R$. Next we consider the first integral of eq. (11), which is illustrated in Fig. 2(a). Here the upgoing field $p^-(\mathbf{x}_R, \omega)$ is backpropagated by the focusing function $F(\mathbf{x}, \mathbf{x}_R, \omega)$ from all $\mathbf{x}_R$ at $\partial\mathbb{D}_R$ to $\mathbf{x}$ in the lower half-space. The sum of the two integrals gives the wave field $p(\mathbf{x}, \omega)$ in the lower half-space. This is a modified form of Huygens' principle, with the focal points $\mathbf{x}_R$ denoting the positions of the secondary sources at $\partial\mathbb{D}_R$, and with the forward and backward propagating focusing functions replacing the Green's functions in the usual form of Huygens' principle. Note that the two integrals cannot be separately associated with $p^+(\mathbf{x}, \omega)$ and $p^-(\mathbf{x}, \omega)$ in the lower half-space; only the sum of the two integrals gives the total field $p(\mathbf{x}, \omega)$, according to eq. (11).

The underlying assumption in the derivation of eq. (11) is that evanescent waves can be neglected at $\partial\mathbb{D}_R$. Hence, it only holds for waves that are propagating at $\partial\mathbb{D}_R$, having a horizontal slowness $\mathbf{s}$ obeying

$$|\mathbf{s}| \leq 1/c_0, \quad \text{at } \partial\mathbb{D}_R. \tag{12}$$

This implies that the foci (and hence the secondary sources) at $\partial\mathbb{D}_R$ are not ideal delta functions [as formulated by eq. (9)] but band-limited versions of delta functions. Note that ignoring evanescent waves at $\partial\mathbb{D}_R$ does not imply that evanescent waves are not accounted for inside the

inhomogeneous medium below $\partial\mathbb{D}_R$. For example, in an isotropic horizontally layered medium with depth-dependent velocity $c(x_3)$, in which the horizontal slowness is independent of depth, waves that are propagating at $\partial\mathbb{D}_R$ become evanescent when they reach a depth at which $1/c(x_3) < |\mathbf{s}| \leq 1/c_0$. In Section 3.4, we show with a numerical example that eq. (11) indeed accounts for such evanescent waves. Although for laterally varying media we cannot formulate a similar precise condition for waves becoming evanescent, it is still true that eq. (11) holds for evanescent waves inside the medium, as long as they are related to propagating waves at the surface, as formulated by eq. (12).

Note that we previously derived a representation similar to eq. (11) with heuristic arguments, and used it as the starting point for deriving the Marchenko method (Wapenaar *et al.* 2013). However, further on in that derivation we applied up/down decomposition to the wave field at an artificial internal boundary in the lower half-space and we neglected evanescent waves throughout space. In the following derivations we avoid up/down decomposition in the lower half-space and evanescent waves are only neglected at $\partial\mathbb{D}_R$. From eq. (11) we derive Green's function representations for the full wave field at any point $\mathbf{x}$ in the subsurface, expressed in terms of the reflection response at the surface.

3 ACOUSTIC GREEN'S FUNCTION REPRESENTATIONS

3.1 Representation for the acoustic dipole Green's function

We introduce the Green's function $G(\mathbf{x}, \mathbf{x}_S, t)$ as a solution of eq. (3) for an impulsive monopole source of volume-injection rate density at $\mathbf{x}_S$, hence

$$\partial_i(\vartheta_{ij}\partial_j G) - \kappa\partial_t^2 G = -\delta(\mathbf{x} - \mathbf{x}_S)\partial_t\delta(t). \tag{13}$$

We demand that G is the causal solution of this equation, hence $G(\mathbf{x}, \mathbf{x}_S, t) = 0$ for $t < 0$. Note that G obeys source–receiver reciprocity, that is $G(\mathbf{x}, \mathbf{x}_S, t) = G(\mathbf{x}_S, \mathbf{x}, t)$. In the frequency domain, $G(\mathbf{x}, \mathbf{x}_S, \omega)$ obeys the following wave equation

$$\mathcal{L}G = i\omega\delta(\mathbf{x} - \mathbf{x}_S). \tag{14}$$

We choose $\mathbf{x}_S = (\mathbf{x}_{H,S}, x_{3,S})$ in the upper half-space, at a vanishing distance ϵ above $\partial\mathbb{D}_R$, hence, $x_{3,S} = x_{3,R} - \epsilon$. We define a dipole-source response as

$$\Gamma(\mathbf{x}, \mathbf{x}_S, \omega) = -\frac{2}{i\omega\rho_0}\partial_{3,S}G(\mathbf{x}, \mathbf{x}_S, \omega), \tag{15}$$

where $\partial_{3,S}$ denotes differentiation with respect to the source coordinate $x_{3,S}$. For $\mathbf{x}$ at $\partial\mathbb{D}_R$ (i.e. just below the source level) we have for the downgoing part

$$\Gamma^+(\mathbf{x}, \mathbf{x}_S, \omega)|_{x_3 = x_{3,R}} = \delta(\mathbf{x}_H - \mathbf{x}_{H,S}). \tag{16}$$

We define the reflection response $R(\mathbf{x}_R, \mathbf{x}_S, \omega)$ of the medium below $\partial\mathbb{D}_R$ as the upgoing part of the dipole-source response $\Gamma(\mathbf{x}_R, \mathbf{x}_S, \omega)$, with $\mathbf{x}_R$ at $\partial\mathbb{D}_R$, hence

$$
\begin{aligned}
R(\mathbf{x}_R, \mathbf{x}_S, \omega) &= \Gamma^-(\mathbf{x}_R, \mathbf{x}_S, \omega) \\
&= -\frac{2}{i\omega\rho_0}\partial_{3,S}G^-(\mathbf{x}_R, \mathbf{x}_S, \omega) \\
&= -\frac{2}{i\omega\rho_0}\partial_{3,S}G^s(\mathbf{x}_R, \mathbf{x}_S, \omega),
\end{aligned}
\tag{17}
$$

where superscript s stands for scattered. Substituting $p(\mathbf{x}, \omega) = \Gamma(\mathbf{x}, \mathbf{x}_S, \omega)$ and $p^\pm(\mathbf{x}_R, \omega) = \Gamma^\pm(\mathbf{x}_R, \mathbf{x}_S, \omega)$ into eq. (11), using eqs (16) and (17), gives

$$\Gamma(\mathbf{x}, \mathbf{x}_S, \omega) = \int_{\partial\mathbb{D}_R} F(\mathbf{x}, \mathbf{x}_R, \omega)R(\mathbf{x}_R, \mathbf{x}_S, \omega)\mathrm{d}\mathbf{x}_R + F^*(\mathbf{x}, \mathbf{x}_S, \omega), \quad \text{for} \quad x_3 \geq x_{3,R}. \tag{18}$$

This is a representation for the dipole response $\Gamma(\mathbf{x}, \mathbf{x}_S, \omega)$ at virtual receiver position $\mathbf{x}$ anywhere in the half-space below $\partial\mathbb{D}_R$, expressed in terms of the reflection response $R(\mathbf{x}_R, \mathbf{x}_S, \omega)$ at $\partial\mathbb{D}_R$. It is similar to our earlier derived Green's function representations for the Marchenko method, but here it has been derived without applying decomposition in the lower half-space. It only excludes the contribution from waves that are evanescent at $\partial\mathbb{D}_R$. Another difference with our earlier representations is that the Green's function on the left-hand side is a dipole response instead of a monopole response. We address this in Section 3.2.

It may be counter intuitive that in eq. (18) we use focusing functions $F(\mathbf{x}, \mathbf{x}_R, \omega)$ and $F^*(\mathbf{x}, \mathbf{x}_S, \omega)$, with their focal points $\mathbf{x}_R$ and $\mathbf{x}_S$ situated at the surface $\partial\mathbb{D}_R$. This is different from the focusing functions in the classical representations for the Marchenko method, which have their focal points in the subsurface. For an intuitive explanation of the right-hand side of eq. (18) we refer again to Fig. 2, this time with $p^+(\mathbf{x}_R, \omega)$ and $p^-(\mathbf{x}_R, \omega)$ replaced by $\delta(\mathbf{x}_{H,R} - \mathbf{x}_{H,S})$ and $R(\mathbf{x}_R, \mathbf{x}_S, \omega)$, respectively. In a similar way as in Section 2, the focusing functions propagate the downgoing source field at $\mathbf{x}_S$ and the upgoing reflection response at $\mathbf{x}_R$ from $\partial\mathbb{D}_R$ to $\mathbf{x}$ in the lower half-space, with the focal points acting again as secondary sources in a modified form of Huygens' principle. The sum of the two integrals gives $\Gamma(\mathbf{x}, \mathbf{x}_S, \omega)$.

3.2 Representation for the acoustic monopole Green's function

In this section we turn eq. (18) into a representation for the monopole Green's function $G(\mathbf{x}, \mathbf{x}_S, \omega)$. To this end we introduce a modified focusing function $f(\mathbf{x}, \mathbf{x}_R, \omega)$ via

$$F(\mathbf{x}, \mathbf{x}_R, \omega) = \frac{2}{i\omega\rho_0} \partial_{3,R} f(\mathbf{x}, \mathbf{x}_R, \omega), \tag{19}$$

where $\partial_{3,R}$ denotes differentiation with respect to $x_{3,R}$. According to eqs (8), (9) and (19), $f(\mathbf{x}, \mathbf{x}_R, \omega)$ obeys the wave equation

$$\mathcal{L}f = 0, \tag{20}$$

the focusing condition

$$\partial_{3,R} f(\mathbf{x}, \mathbf{x}_R, \omega)|_{x_3 = x_{3,R}} = \frac{i\omega\rho_0}{2} \delta(\mathbf{x}_\mathrm{H} - \mathbf{x}_{\mathrm{H},R}), \tag{21}$$

and it is upgoing at and above $\partial\mathbb{D}_R$. Eq. (19) implies

$$F^*(\mathbf{x}, \mathbf{x}_S, \omega) = -\frac{2}{i\omega\rho_0} \partial_{3,S} f^*(\mathbf{x}, \mathbf{x}_S, \omega). \tag{22}$$

Substituting eqs (15), (17), (19) and (22) into eq. (18), applying source–receiver reciprocity to the scattered Green's function and dropping the operation $-\frac{2}{i\omega\rho_0}\partial_{3,S}$ from all terms gives

$$G(\mathbf{x}, \mathbf{x}_S, \omega) = \frac{2}{i\omega\rho_0} \int_{\partial\mathbb{D}_R} \{\partial_{3,R} f(\mathbf{x}, \mathbf{x}_R, \omega)\} G^\mathrm{s}(\mathbf{x}_S, \mathbf{x}_R, \omega) \mathrm{d}\mathbf{x}_R + f^*(\mathbf{x}, \mathbf{x}_S, \omega), \quad \text{for} \quad x_3 \geq x_{3,R}. \tag{23}$$

We transfer the operator $\partial_{3,R}$ from f to G^s, which is accompanied with a sign change (see Appendix A2). Using the definition of R in eq. (17) (with $\partial_{3,S}$ replaced by $\partial_{3,R}$ and with $\mathbf{x}_R$ and $\mathbf{x}_S$ interchanged on both sides of the equation) this yields

$$G(\mathbf{x}, \mathbf{x}_S, \omega) = \int_{\partial\mathbb{D}_R} f(\mathbf{x}, \mathbf{x}_R, \omega) R(\mathbf{x}_S, \mathbf{x}_R, \omega) \mathrm{d}\mathbf{x}_R + f^*(\mathbf{x}, \mathbf{x}_S, \omega), \quad \text{for} \quad x_3 \geq x_{3,R}. \tag{24}$$

This is the main result of this paper. We discuss a number of aspects of this representation.

(i) Eq. (24) has the same form as eq. (13) in Wapenaar *et al.* (2014), with f_2 in that paper replaced by f. Using $\partial_{3,R} f(\mathbf{x}, \mathbf{x}_R, \omega) = -\partial_3 f(\mathbf{x}, \mathbf{x}_R, \omega)$ for $x_3 = x_{3,R}$ (i.e. at the boundary of the homogeneous upper half-space), eq. (21) can be written as

$$\partial_3 f(\mathbf{x}, \mathbf{x}_R, \omega)|_{x_3 = x_{3,R}} = -\frac{i\omega\rho_0}{2} \delta(\mathbf{x}_\mathrm{H} - \mathbf{x}_{\mathrm{H},R}). \tag{25}$$

This is the same focusing condition as was defined for $f_2(\mathbf{x}, \mathbf{x}_R, \omega)$. An important difference between f and f_2 is the medium in which these focusing functions are defined. Focusing function f_2 is defined in a truncated version of the actual medium, where the medium below some depth level is replaced by a homogeneous medium. It is assumed that up/down decomposition is possible at the truncation level. On the other hand, focusing function f in eq. (24) is defined in the actual medium (similar as F in Fig. 1).
Moreover, the derivation in Wapenaar *et al.* (2014) of the representation is different: in that paper we start with decomposed focusing functions $f_1^+(\mathbf{x}, \mathbf{x}_A, \omega)$ and $f_1^-(\mathbf{x}, \mathbf{x}_A, \omega)$ in the truncated medium, with $\mathbf{x}_A$ being a focal point at the truncation depth. Next, we derive representations for decomposed Green's functions $G^+(\mathbf{x}_A, \mathbf{x}_S, \omega)$ and $G^-(\mathbf{x}_A, \mathbf{x}_S, \omega)$ and combine the two into a single representation for $G(\mathbf{x}_A, \mathbf{x}_S, \omega) = G^+(\mathbf{x}_A, \mathbf{x}_S, \omega) + G^-(\mathbf{x}_A, \mathbf{x}_S, \omega)$, using the relation $f_2(\mathbf{x}_A, \mathbf{x}_R, \omega) = f_1^+(\mathbf{x}_R, \mathbf{x}_A, \omega) - \{f_1^-(\mathbf{x}_R, \mathbf{x}_A, \omega)\}^*$ (note the different order of coordinates in f_1 and f_2). The latter relation is only valid when evanescent waves can be neglected at the truncation level inside the medium. In our current approach we do not make use of decomposition at a truncation level inside the medium and we avoid the approximate relation $f_2 = f_1^+ - \{f_1^-\}^*$. The only requirement for $f(\mathbf{x}, \mathbf{x}_R, \omega)$ is that it obeys eqs (20) and (21). Hence, representation (24) gives the full wave field at the virtual receiver position $\mathbf{x}$ inside the medium, including multiply reflected, refracted and evanescent waves. It only excludes the contribution from waves that are evanescent at $\partial\mathbb{D}_R$, see the condition formulated by eq. (12).

(ii) Using another approach, also without applying decomposition inside the medium, Diekmann & Vasconcelos (2021) derive an equation of the same form as eq. (24), but without specifying a focusing condition for f. Their focusing function obeys a wave equation with a non-zero time-symmetric source function which is not explicitly specified. The derivation of eq. (24) in the current paper uses an explicit focusing condition (eq. 21) and does not require a source function for f.

(iii) Eq. (24) forms a starting point for deriving the Marchenko method. By applying an inverse Fourier transform we obtain

$$G(\mathbf{x}, \mathbf{x}_S, t) - f(\mathbf{x}, \mathbf{x}_S, -t) = \int_{\partial\mathbb{D}_R} \mathrm{d}\mathbf{x}_R \int_{-\infty}^t f(\mathbf{x}, \mathbf{x}_R, t') R(\mathbf{x}_S, \mathbf{x}_R, t - t') \mathrm{d}t', \quad \text{for} \quad x_3 \geq x_{3,R}. \tag{26}$$

The Marchenko method is based on the separability in time of $G(\mathbf{x}, \mathbf{x}_S, t)$ and $f(\mathbf{x}, \mathbf{x}_S, -t)$. For horizontal plane waves in 1-D media (Burridge 1980; Broggini & Snieder 2012) and for point-source responses at limited horizontal distances $|\mathbf{x}_\mathrm{H} - \mathbf{x}_{\mathrm{H},S}|$ in moderately inhomogeneous 3-D media (Wapenaar *et al.* 2013), these functions only overlap at $t = t_\mathrm{d}$, which is the time of the direct arrival of the Green's function. This minimum overlap in time allows the construction of a time-windowed version of eq. (26) with $G(\mathbf{x}, \mathbf{x}_S, t)$ suppressed and with $f(\mathbf{x}, \mathbf{x}_S, -t)$ almost completely preserved (this is the 3-D Marchenko equation). From this equation the focusing function $f(\mathbf{x}, \mathbf{x}_S, t)$ can be resolved, given

its direct arrival and the reflection response $R(\mathbf{x}_S, \mathbf{x}_R, t)$. In essence the separability of the Green's function and the time-reversed focusing function has been the underlying assumption of all implementations of the Marchenko method. This assumption excludes, among others, the treatment of refracted waves, which may arrive prior to the direct arrival of the Green's function and interfere with the time-reversed focusing function.

Since we have argued that the representations of eqs (24) and (26) hold for refracted and evanescent waves, it is opportune to start new research on Marchenko methods which exploit the generality of these representations. Care should be taken to account for the overlap in time of the Green's function and the time-reversed focusing function, particularly when dealing with refracted waves. A further discussion of the development of new Marchenko methods is beyond the scope of this paper.

(iv) Eq. (24) is, in principle, suited to retrieve the Green's function $G(\mathbf{x}, \mathbf{x}_S, \omega)$ for $\mathbf{x}$ anywhere in the lower half-space. However, a single type of Green's function is not a sufficient starting point for imaging. In the classical approach to Marchenko imaging, the downgoing and upgoing parts of the Green's function are retrieved, from which a reflection image can be obtained, either by a deconvolution (Broggini *et al.* 2014; Wapenaar *et al.* 2014) or a correlation method (Behura *et al.* 2014). In the full-wavefield approach, we need at least one other type of field at $\mathbf{x}$, next to $G(\mathbf{x}, \mathbf{x}_S, \omega)$, which represents the acoustic pressure field at $\mathbf{x}$ in response to a volume-injection rate source at $\mathbf{x}_S$. To this end we introduce a Green's function $G_i^v(\mathbf{x}, \mathbf{x}_S, \omega)$ which, for $i = 1, 2$ and 3, stands for the three components of the particle velocity field at $\mathbf{x}$. From the Fourier transform of eq. (1) we derive that the particle velocity v_i can be expressed in terms of the acoustic pressure as $v_i = \frac{1}{i\omega}\vartheta_{ij}\partial_j p$. Similarly, we relate G_i^v to G via

$$G_i^v(\mathbf{x}, \mathbf{x}_S, \omega) = \frac{1}{i\omega}\vartheta_{ij}(\mathbf{x})\partial_j G(\mathbf{x}, \mathbf{x}_S, \omega). \tag{27}$$

Hence, when $G(\mathbf{x}, \mathbf{x}_S, \omega)$ is available on a sufficiently dense grid, $G_i^v(\mathbf{x}, \mathbf{x}_S, \omega)$ can be obtained via eq. (27). Alternatively, $G_i^v(\mathbf{x}, \mathbf{x}_S, \omega)$ can be obtained from a modified version of the representation for $G(\mathbf{x}, \mathbf{x}_S, \omega)$. Applying the operation $\frac{1}{i\omega}\vartheta_{ij}\partial_j$ to both sides of eq. (24) yields

$$G_i^v(\mathbf{x}, \mathbf{x}_S, \omega) = \int_{\partial\mathbb{D}_R} h_i(\mathbf{x}, \mathbf{x}_R, \omega)R(\mathbf{x}_S, \mathbf{x}_R, \omega)\mathrm{d}\mathbf{x}_R - h_i^*(\mathbf{x}, \mathbf{x}_S, \omega), \quad \text{for} \quad x_3 \geq x_{3,R}, \tag{28}$$

with

$$h_i(\mathbf{x}, \mathbf{x}_R, \omega) = \frac{1}{i\omega}\vartheta_{ij}(\mathbf{x})\partial_j f(\mathbf{x}, \mathbf{x}_R, \omega). \tag{29}$$

The Green's functions $G(\mathbf{x}, \mathbf{x}_S, \omega)$ and $G_i^v(\mathbf{x}, \mathbf{x}_S, \omega)$ together provide sufficient information for imaging. For example, one could decompose the field into incident and scattered waves in any desired direction, say in a direction perpendicular to a local interface (Yoon & Marfurt 2006; Liu *et al.* 2011; Holicki *et al.* 2019), and use these fields as input for imaging.

3.3 Representation for the homogeneous acoustic Green's function

The representations in Sections 3.1 and 3.2 give the response to a source at $\mathbf{x}_S$, observed by a virtual receiver at $\mathbf{x}$ inside the medium. Here we modify the representation of eq. (24), to create the response at the surface to a virtual source inside the medium. After that, we show how to obtain the response to this virtual source at a virtual receiver inside the medium.

We start by renaming the coordinate vectors in eq. (24) as follows: $\mathbf{x}_S \to \mathbf{x}_R, \mathbf{x}_R \to \mathbf{x}_S, \mathbf{x} \to \mathbf{x}_A$. This yields, in combination with applying source–receiver reciprocity on the left-hand side of eq. (24),

$$G(\mathbf{x}_R, \mathbf{x}_A, \omega) = \int_{\partial\mathbb{D}_R} R(\mathbf{x}_R, \mathbf{x}_S, \omega)f(\mathbf{x}_A, \mathbf{x}_S, \omega)\mathrm{d}\mathbf{x}_S + f^*(\mathbf{x}_A, \mathbf{x}_R, \omega), \text{ for} \quad x_{3,A} \geq x_{3,R}. \tag{30}$$

Here $R(\mathbf{x}_R, \mathbf{x}_S, \omega)$ is the reflection response to a dipole source at $\mathbf{x}_S$, observed by a receiver at $\mathbf{x}_R$, both at the surface $\partial\mathbb{D}_R$. This is schematically illustrated in Fig. 3(a). The integral in eq. (30) describes redatuming of the sources from all $\mathbf{x}_S$ at the surface to virtual-source position $\mathbf{x}_A$ in the subsurface, see Fig. 3(b). After adding $f^*(\mathbf{x}_A, \mathbf{x}_R, \omega)$ (according to eq. 30) this gives the Green's function $G(\mathbf{x}_R, \mathbf{x}_A, \omega)$, which is the response to the virtual monopole source at $\mathbf{x}_A$, observed by the receiver at $\mathbf{x}_R$ at the surface.

Our next aim is to derive a representation for the response observed by a virtual receiver at $\mathbf{x}$ in the subsurface, given $G(\mathbf{x}_R, \mathbf{x}_A, \omega)$. Eq. (11) cannot be used for this in the same way as before, since $G(\mathbf{x}, \mathbf{x}_A, \omega)$ obeys a wave equation with a singularity at $\mathbf{x}_A$, whereas $p(\mathbf{x}, \omega)$ in eq. (11) is not allowed to have sources in the lower half-space. To overcome this problem, we define the homogeneous Green's function (Porter 1970; Oristaglio 1989)

$$G_{\mathrm{h}}(\mathbf{x}, \mathbf{x}_A, \omega) = G(\mathbf{x}, \mathbf{x}_A, \omega) + G^*(\mathbf{x}, \mathbf{x}_A, \omega). \tag{31}$$

Here $G(\mathbf{x}, \mathbf{x}_A, \omega)$ and $G^*(\mathbf{x}, \mathbf{x}_A, \omega)$ obey eq. (14), with source terms $i\omega\delta(\mathbf{x} - \mathbf{x}_A)$ and $-i\omega\delta(\mathbf{x} - \mathbf{x}_A)$, respectively, on the right-hand sides. Hence, $G_{\mathrm{h}}(\mathbf{x}, \mathbf{x}_A, \omega)$ obeys the following equation:

$$\mathcal{L}G_{\mathrm{h}} = 0, \tag{32}$$

which confirms that the homogeneous Green's function is source-free. This time we choose for $p(\mathbf{x}, \omega)$ in eq. (11)

$$p(\mathbf{x}, \omega) = G_{\mathrm{h}}(\mathbf{x}, \mathbf{x}_A, \omega), \tag{33}$$
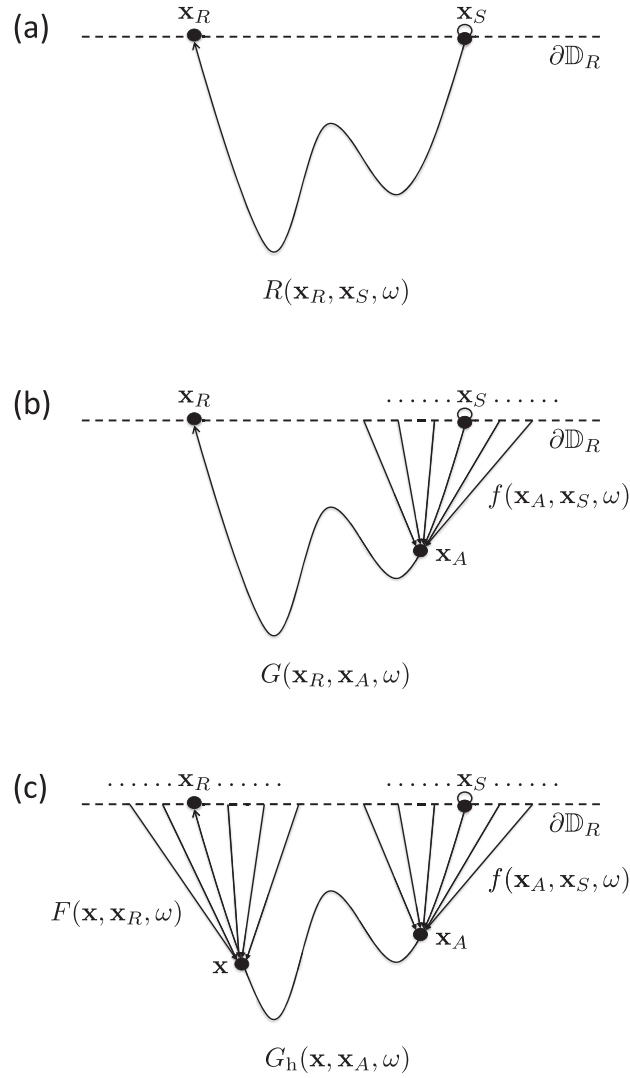
Figure 3. Illustration of source and receiver redatuming as a two-step process. Starting with (a) the reflection response $R(\mathbf{x}_R, \mathbf{x}_S, \omega)$ at the surface, in step one (b) the Green's function $G(\mathbf{x}_R, \mathbf{x}_A, \omega)$ is obtained for a virtual source at $\mathbf{x}_A$, and step two (c) yields the homogeneous Green's function $G_h(\mathbf{x}, \mathbf{x}_A, \omega)$ for a virtual receiver at $\mathbf{x}$. All functions in this figure are represented by simple rays, but in reality these are wave fields, including primaries, multiples, refracted and evanescent waves.

with $G_h(\mathbf{x}, \mathbf{x}_A, \omega)$ defined in eq. (31). For $\mathbf{x}$ at $\partial\mathbb{D}_R$ the Green's function $G(\mathbf{x}, \mathbf{x}_A, \omega)$ is purely upgoing, since the upper half-space is homogeneous and the virtual source at $\mathbf{x}_A$ lies in the lower half-space. Similarly, $G^*(\mathbf{x}, \mathbf{x}_A, \omega)$ is downgoing at $\partial\mathbb{D}_R$, except for the evanescent field [which we already neglected at $\partial\mathbb{D}_R$ in the derivation of eq. (11)]. Hence, we may write

$$p^-(\mathbf{x}, \omega) = G_h^-(\mathbf{x}, \mathbf{x}_A, \omega) = G(\mathbf{x}, \mathbf{x}_A, \omega), \quad \text{for} \quad x_3 = x_{3,R}, \tag{34}$$

$$p^+(\mathbf{x}, \omega) = G_h^+(\mathbf{x}, \mathbf{x}_A, \omega) = G^*(\mathbf{x}, \mathbf{x}_A, \omega), \quad \text{for} \quad x_3 = x_{3,R}. \tag{35}$$

Substitution of eqs (33)–(35) into eq. (11) yields

$$G_h(\mathbf{x}, \mathbf{x}_A, \omega) = \int_{\partial\mathbb{D}_R} F(\mathbf{x}, \mathbf{x}_R, \omega) G(\mathbf{x}_R, \mathbf{x}_A, \omega) d\mathbf{x}_R + \int_{\partial\mathbb{D}_R} F^*(\mathbf{x}, \mathbf{x}_R, \omega) G^*(\mathbf{x}_R, \mathbf{x}_A, \omega) d\mathbf{x}_R, \quad \text{for} \quad x_3 \geq x_{3,R}, \tag{36}$$

or

$$G_h(\mathbf{x}, \mathbf{x}_A, \omega) = 2\Re \int_{\partial\mathbb{D}_R} F(\mathbf{x}, \mathbf{x}_R, \omega) G(\mathbf{x}_R, \mathbf{x}_A, \omega) d\mathbf{x}_R, \quad \text{for} \quad x_3 \geq x_{3,R}, \tag{37}$$

where $\Re$ denotes that the real part is taken. For an intuitive explanation of the right-hand side of eq. (36) we refer again to Fig. 2, this time with $p^+(\mathbf{x}_R, \omega)$ and $p^-(\mathbf{x}_R, \omega)$ replaced by $G^*(\mathbf{x}_R, \mathbf{x}_A, \omega)$ and $G(\mathbf{x}_R, \mathbf{x}_A, \omega)$, respectively. The focusing functions propagate these downgoing and upgoing Green's functions at $\mathbf{x}_R$ from $\partial\mathbb{D}_R$ into the lower half-space, with the focal points acting as secondary sources in a modified form

of Huygens' principle. The two integrals cannot be separately associated with $G^*(\mathbf{x}, \mathbf{x}_A, \omega)$ and $G(\mathbf{x}, \mathbf{x}_A, \omega)$ for $\mathbf{x}$ in the lower half-space (these functions are singular at $\mathbf{x}_A$); only the sum of the two integrals gives $G_\mathrm{h}(\mathbf{x}, \mathbf{x}_A, \omega)$ (which is not singular at $\mathbf{x}_A$).

Hence, eq. (36) describes redatuming of the receivers from all $\mathbf{x}_R$ at the surface to virtual-receiver position $\mathbf{x}$ in the subsurface, see Fig. 3(c). It gives the homogeneous Green's function $G_\mathrm{h}(\mathbf{x}, \mathbf{x}_A, \omega)$, which is the response to the virtual source at $\mathbf{x}_A$, observed by a virtual receiver at $\mathbf{x}$, plus its complex conjugate. After transforming this to the time domain we obtain

$$G_\mathrm{h}(\mathbf{x}, \mathbf{x}_A, t) = G(\mathbf{x}, \mathbf{x}_A, t) + G(\mathbf{x}, \mathbf{x}_A, -t). \tag{38}$$

The two functions at the right-hand side of this equation do not overlap in time (except for $\mathbf{x} = \mathbf{x}_A$ and only for $t = 0$), hence, $G(\mathbf{x}, \mathbf{x}_A, t)$ can be extracted from $G_\mathrm{h}(\mathbf{x}, \mathbf{x}_A, t)$ by selecting its causal part.

Note that there is an asymmetry in the focusing functions used for source redatuming [$f(\mathbf{x}_A, \mathbf{x}_S, \omega)$ in eq. (30)] and for receiver redatuming [$F(\mathbf{x}, \mathbf{x}_R, \omega)$ in eq. (37)], see also Fig. 3(c). This is due to the difference in types of responses at the surface [the dipole response $R(\mathbf{x}_R, \mathbf{x}_S, \omega)$] and in the subsurface [the monopole response $G(\mathbf{x}, \mathbf{x}_A, \omega)$]. When the response at the surface were also a monopole response, then the focusing function $f(\mathbf{x}_A, \mathbf{x}_S, \omega)$ for source redatuming should be replaced by $F(\mathbf{x}_A, \mathbf{x}_S, \omega)$.

Homogeneous Green's function representations similar to eq. (37) were also derived by Wapenaar *et al.* (2016a), van der Neut *et al.* (2017) and Singh & Snieder (2017), but here eq. (37) has been derived without up/down decomposition inside the medium. Hence, it also holds for evanescent waves inside the medium, as long as condition (12) is obeyed. Moreover, the derivation presented here is much simpler than in those references.

The source and receiver redatuming processes can be captured in one equation by substituting eq. (30) into (37). This gives

$$G_\mathrm{h}(\mathbf{x}, \mathbf{x}_A, \omega) = 2\Re \int_{\partial \mathbb{D}_R} \int_{\partial \mathbb{D}_R} F(\mathbf{x}, \mathbf{x}_R, \omega) R(\mathbf{x}_R, \mathbf{x}_S, \omega) f(\mathbf{x}_A, \mathbf{x}_S, \omega) \mathrm{d}\mathbf{x}_S \mathrm{d}\mathbf{x}_R$$

$$+ 2\Re \int_{\partial \mathbb{D}_R} F(\mathbf{x}, \mathbf{x}_R, \omega) f^*(\mathbf{x}_A, \mathbf{x}_R, \omega) \mathrm{d}\mathbf{x}_R, \quad \text{for} \quad \{x_3, x_{3,A}\} \geq x_{3,R}. \tag{39}$$

The double integral on the right-hand side resembles the process of classical source and receiver redatuming (Berkhout 1982; Berryhill 1984), but with the primary focusing functions in those references replaced by full-field focusing functions. It also resembles source–receiver interferometry (Curtis & Halliday 2010), but with the double integration along a closed boundary in that paper replaced by the double integration over the open boundary $\partial \mathbb{D}_R$. Hence, via the theories of primary source–receiver redatuming (Berkhout 1982; Berryhill 1984), closed-boundary source–receiver interferometry (Curtis & Halliday 2010) and open-boundary homogeneous Green's function retrieval using wave field decomposition (Wapenaar *et al.* 2016a; van der Neut *et al.* 2017; Singh & Snieder 2017), we have arrived at a representation for open-boundary homogeneous full-field Green's function retrieval (eq. 39), which accounts for internal multiples, and refracted and evanescent waves in the lower half-space. In Section 5.3 this representation is extended for the elastodynamic situation.

3.4 Numerical examples

We illustrate the representations of Sections 3.2 and 3.3 with numerical examples. Our main aim is to demonstrate that these representations hold for evanescent waves inside the medium. To this end we consider oblique plane waves in a horizontally layered medium, with isotropic depth-dependent medium parameters $c(x_3)$ (propagation velocity) and $\rho(x_3)$ (mass density). We consider a horizontally layered medium because in this case we can unequivocally distinguish between propagating and evanescent waves. However, as discussed in Section 2, the representations also account for evanescent waves in more general inhomogeneous media. We define the spatial Fourier transform of a space- and frequency-dependent function $u(\mathbf{x}, \omega)$ as

$$\tilde{u}(\mathbf{s}, x_3, \omega) = \int_{\mathbb{R}^2} \exp\{-i\omega \mathbf{s} \cdot \mathbf{x}_\mathrm{H}\} u(\mathbf{x}_\mathrm{H}, x_3, \omega) \mathrm{d}\mathbf{x}_\mathrm{H}, \tag{40}$$

with $\mathbf{s} = (s_1, s_2)$, where s_1 and s_2 are horizontal slownesses and $\mathbb{R}$ is the set of real numbers. This decomposes the function $u(\mathbf{x}, \omega)$ into monochromatic plane-wave components. Next, we define the inverse temporal Fourier transform per slowness value as

$$u(\mathbf{s}, x_3, \tau) = \frac{1}{\pi} \Re \int_0^\infty \tilde{u}(\mathbf{s}, x_3, \omega) \exp\{-i\omega \tau\} \mathrm{d}\omega, \tag{41}$$

where τ is the so-called intercept time (Stoffa 1989).

First we investigate the representation of eq. (24) and take $\mathbf{x}_S = (0, 0, x_{3,R})$. We use the definitions of eqs (40) and (41) to transform this representation to the slowness intercept-time domain. Taking into account that for a horizontally layered, isotropic medium all functions in eq. (24) are cylindrically symmetric, it suffices to consider the transformed representation for one slowness variable only. We thus obtain

$$G(s_1, x_3, x_{3,R}, \tau) = \int_{-\infty}^\tau f(s_1, x_3, x_{3,R}, \tau') R(s_1, x_{3,R}, \tau - \tau') \mathrm{d}\tau' + f(s_1, x_3, x_{3,R}, -\tau), \quad \text{for} \quad x_3 \geq x_{3,R}. \tag{42}$$

For any given value of s_1, the Green's function $G(s_1, x_3, x_{3,R}, \tau)$ is the response to a plane-wave source at $x_{3,R}$ as a function of receiver depth x_3 and intercept time τ. For $|s_1| \leq 1/c(x_3)$ the plane wave is propagating, whereas for $|s_1| > 1/c(x_3)$ it is evanescent. For propagating waves, the local propagation angle $\alpha(x_3)$ follows from $s_1 = \sin \alpha(x_3)/c(x_3)$. The focusing function $f(s_1, x_3, x_{3,R}, \tau)$ obeys the focusing condition
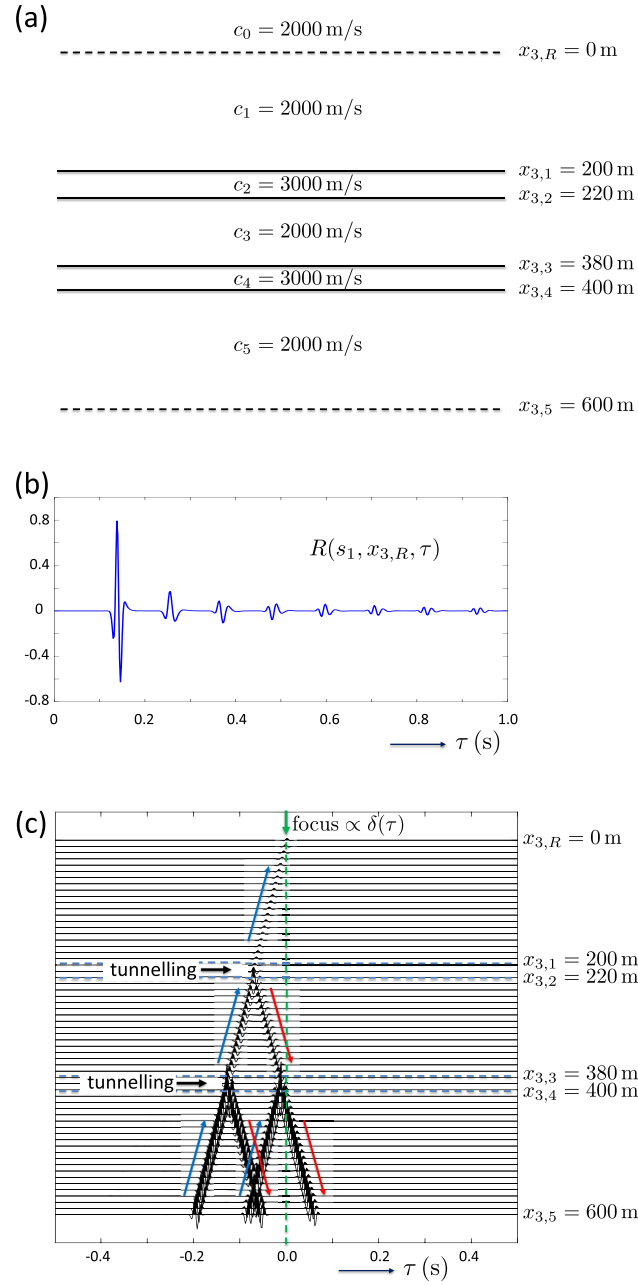
Figure 4. (a) Horizontally layered medium with two high-velocity layers. (b) Numerically modelled reflection response $R(s_1, x_{3,R}, \tau)$ at the surface. The horizontal slowness $s_1 = 1/2800$ s m^{-1} is chosen such that the wave field is evanescent in the high-velocity layers. (c) Numerically modelled focusing function $f(s_1, x_3, x_{3,R}, \tau)$. The trace at $x_{3,R} = 0$ m illustrates the focusing condition of eq. (43).

formulated by eq. (25), transformed to the slowness intercept-time domain, hence

$$f(s_1, x_3, x_{3,R}, \tau)|_{x_3=x_{3,R}} = \frac{\rho_0 c_0}{2 \cos \alpha_0} \delta(\tau), \tag{43}$$

with $\alpha_0 = \alpha(x_{3,R})$. Consider the horizontally layered medium of Fig. 4(a). Two thin high-velocity layers ($c_2 = c_4 = 3000$ m s^{-1}) are embedded in a homogeneous background medium with a velocity of 2000 m s^{-1}. The mass densities, in kg m^{-3}, are assigned the same numerical values as the velocities to get significant contrasts between the different layers. A plane wave is emitted from $x_{3,R}$ into the medium, with slowness $s_1 = 1/2800$ s m^{-1}, hence, this wave leaves the surface with an angle $\alpha_0 = 45.6°$ and becomes evanescent in the high-velocity layers. For the source function we use a Ricker wavelet with a central frequency of 50 Hz, hence, the wavelength for the central frequency in the high-velocity layers is 60 m. The thickness of the high-velocity layers is 20 m, which is of the same order as the distance over which the evanescent waves decay with a factor $1/e$, which is equal to $1/(\omega_c\sqrt{s_1^2 - 1/c_2^2})$=24.8 m. Hence, we may expect that the waves tunnel through these layers. Fig. 4(b) shows the numerically modelled reflection response $R(s_1, x_{3,R}, \tau)$ for the chosen slowness. The first two events are composite reflections from the two high-velocity layers (including internal multiples of evanescent waves inside these layers) and the other events are multiple reflections

between these layers. Fig. 4(c) shows the numerically modelled focusing function $f(s_1, x_3, x_{3,R}, \tau)$ as a function of x_3 and τ, convolved with the same Ricker wavelet for a clear display. Blue and red arrows indicate upgoing and downgoing waves, respectively, in the homogeneous background medium. The tunnelling of the waves through the high-velocity layers is clearly visible. A single upgoing wave reaches the surface $x_{3,R}$ at $\tau = 0$, conform the focusing condition formulated by eq. (43) [except that in this display $\delta(\tau)$ is convolved with the Ricker wavelet]. Note that the amplitude increases with increasing depth (to compensate for the evanescent waves in the high-velocity layers), which means that, in practice, the numerically computed focusing function becomes unstable beyond some thickness of the high-velocity layers.

The reflection response of Fig. 4(b) and the focusing function of Fig. 4(c) (the latter without the wavelet) are used as input for the representation of eq. (42). This yields the Green's function $G(s_1, x_3, x_{3,R}, \tau)$ (convolved with the Ricker wavelet) as a function of x_3 and τ, see Fig. 5(a). Blue and red arrows indicate again upgoing and downgoing waves, respectively. This figure shows the expected behaviour of the response to a plane-wave source at $x_{3,R}$ (a downgoing wave leaving the surface, two composite primary upgoing waves and multiple reflections between the high velocity layers). Fig. 5(b) shows $G(s_1, x_{3,A}, x_{3,R}, \tau)$ for $x_{3,A} = 300$ m. The green line is the Green's function obtained from eq. (42), the red line is the directly modelled Green's function. Similarly, Fig. 5(c) shows $G(s_1, x_{3,B}, x_{3,R}, \tau)$ for $x_{3,B} = 210$ m, that is inside the first high velocity layer. In both cases the match is perfect, which confirms that the representation of eq. (42) correctly accounts for propagating and evanescent waves inside the medium.

Using source–receiver reciprocity we may interpret Fig. 5(b) as $G(s_1, x_{3,R}, x_{3,A}, \tau)$, which is the response at the surface $x_{3,R}$ to a virtual plane-wave source at $x_{3,A} = 300$ m. Hence, $G(s_1, x_{3,R}, x_{3,A}, \tau)$ may be seen as the result of redatuming the source from the surface to $x_{3,A}$. We now discuss receiver redatuming. To this end, we transform the representation of eq. (36) to the slowness intercept-time domain, which yields

$$G_{\mathrm{h}}(s_1, x_3, x_{3,A}, \tau) = \int_{-\infty}^{\tau} F(s_1, x_3, x_{3,R}, \tau') G(s_1, x_{3,R}, x_{3,A}, \tau - \tau') \mathrm{d}\tau'$$
$$+ \int_{\tau}^{\infty} F(s_1, x_3, x_{3,R}, -\tau') G(s_1, x_{3,R}, x_{3,A}, \tau' - \tau) \mathrm{d}\tau', \quad \text{for} \quad x_3 \geq x_{3,R}, \tag{44}$$

with, analogous to eq. (19),

$$F(s_1, x_3, x_{3,R}, \tau) = \frac{2 \cos \alpha_0}{\rho_0 c_0} f(s_1, x_3, x_{3,R}, \tau). \tag{45}$$

Note that the right-hand side of eq. (44) contains the Green's function with the redatumed source at $x_{3,A}$ and the receiver at $x_{3,R}$ at the surface. This representation redatums the receiver from $x_{3,R}$ to any depth x_3 in the subsurface. This yields the homogeneous Green's function, which consists of $G(s_1, x_3, x_{3,A}, \tau)$ plus its time-reversal, see Fig. 5(d). The causal part (right of the green dashed line) is the retrieved Green's function $G(s_1, x_3, x_{3,A}, \tau)$. Conform expectation, we see a virtual source at $x_{3,A}$ emitting downgoing and upgoing plane waves, which reverberate in the wave guide between the two high-velocity layers, but which also emit some energy through tunnelling into the half-spaces above and below the high-velocity layers. This example illustrates the handling of propagating and evanescent waves inside the medium by the homogeneous Green's function representation of eq. (44).

4 ELASTODYNAMIC WAVE FIELD REPRESENTATION

We derive the elastodynamic equivalent of the representation of eq. (11). We consider the same configuration as in Section 2, except that now the medium parameters of the lower half-space $x_3 > x_{3,R}$ are the stiffness tensor $c_{ijkl}(\mathbf{x})$ and the mass density tensor $\rho_{ik}(\mathbf{x})$, with symmetries $c_{ijkl} = c_{jikl} = c_{ijlk} = c_{klij}$ and $\rho_{ik} = \rho_{ki}$. In the homogeneous isotropic upper half-space $x_3 \leq x_{3,R}$ the parameters are $\rho_{ik} = \delta_{ik}\rho_0$ and $c_{ijkl} = \lambda_0 \delta_{ij}\delta_{kl} + \mu_0(\delta_{ik}\delta_{jl} + \delta_{il}\delta_{jk})$, with λ_0 and μ_0 the Lamé parameters of the half-space. The *P*- and *S*-wave propagation velocities of the upper half-space are $c_P = [(\lambda_0 + 2\mu_0)/\rho_0]^{1/2}$ and $c_S = (\mu_0/\rho_0)^{1/2}$, respectively.

The basic equations in the frequency domain for elastodynamic wave propagation are the linearized equation of motion

$$-i\omega\rho_{ik}v_k - \partial_j \tau_{ij} = \hat{f}_i \tag{46}$$

and the linearized deformation equation

$$i\omega\tau_{ij} + c_{ijkl}\partial_l v_k = 0, \tag{47}$$

respectively. Here $\tau_{ij}(\mathbf{x}, \omega)$ is the stress tensor (with symmetry $\tau_{ij} = \tau_{ji}$), $v_k(\mathbf{x}, \omega)$ the particle velocity and $\hat{f}_i(\mathbf{x}, \omega)$ a source in terms of volume-force density (the circumflex is used to distinguish this source term from the focusing function). Eqs (46) and (47) can be combined into the elastodynamic wave equation

$$\mathcal{L}_{ik}v_k = i\omega\hat{f}_i, \tag{48}$$

with

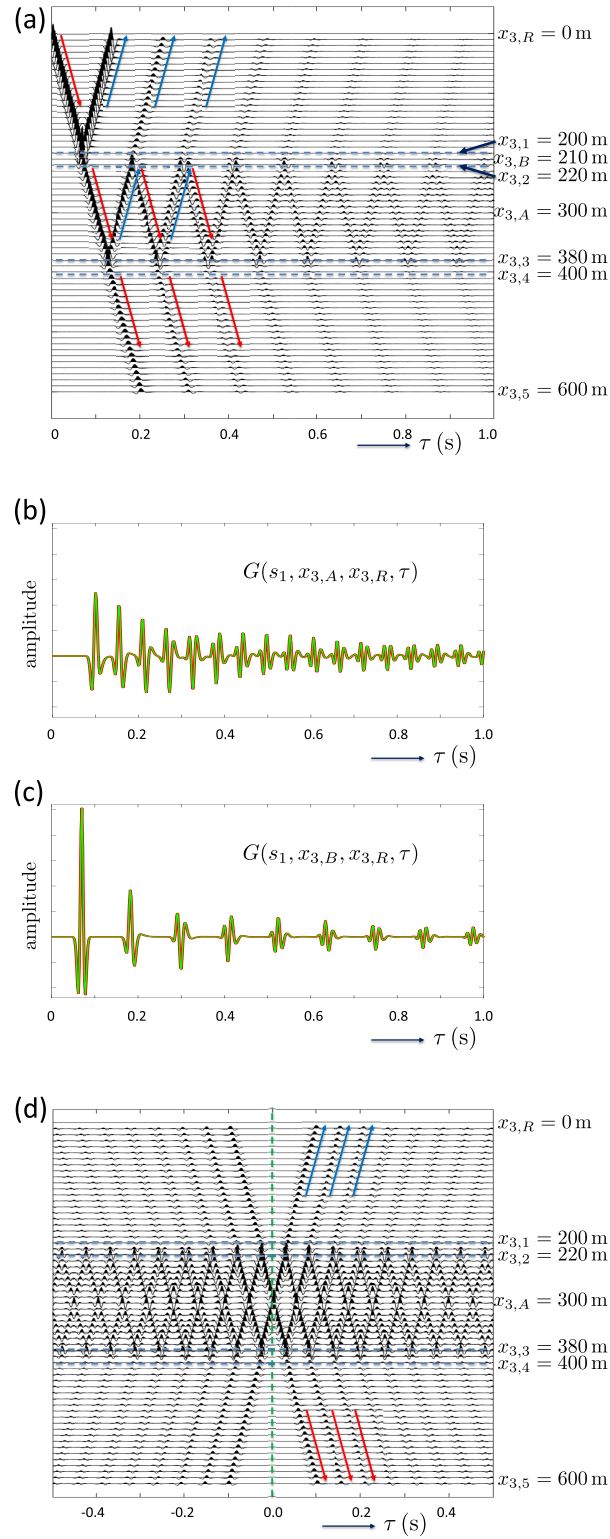$$\mathcal{L}_{ik} = \partial_j c_{ijkl}\partial_l + \omega^2 \rho_{ik}. \tag{49}$$

Figure 5. (a) Green's function $G(s_1, x_3, x_{3,R}, \tau)$ obtained from Figs 4(b) and (c) via the representation of eq. (42). (b) $G(s_1, x_{3,A}, x_{3,R}, \tau)$, taken from figure (a) for $x_{3,A} = 300$ m (green), compared with directly modelled Green's function (red). (c) Similarly, $G(s_1, x_{3,B}, x_{3,R}, \tau)$, taken from figure (a) for $x_{3,B} = 210$ m inside the first high velocity layer. (d) Homogeneous Green's function $G_h(s_1, x_3, x_{3,A}, \tau)$ obtained from Figs 4(c) and 5(b) via the representation of eq. (44).

We introduce an elastodynamic focusing function $\mathbf{F}(\mathbf{x}, \mathbf{x}_R, \omega)$ as a 3×3 matrix, according to

$$\mathbf{F}(\mathbf{x}, \mathbf{x}_R, \omega) = \begin{pmatrix} F_{1,1} & F_{1,2} & F_{1,3} \\ F_{2,1} & F_{2,2} & F_{2,3} \\ F_{3,1} & F_{3,2} & F_{3,3} \end{pmatrix} (\mathbf{x}, \mathbf{x}_R, \omega), \tag{50}$$

where $\mathbf{x}_R$ denotes again the position of a focal point at $\partial \mathbb{D}_R$. Each column of $\mathbf{F}$ is a particle velocity vector of which the components, for fixed $\mathbf{x}_R$ and variable $\mathbf{x}$, obey the elastodynamic wave eq. (48) for the source-free situation. This is different from the elastodynamic focusing function introduced by Wapenaar & Slob (2014), in which the different elements represent decomposed compressional and shear waves.

We define the focusing condition, analogous to eq. (9), as

$$\mathbf{F}(\mathbf{x}, \mathbf{x}_R, \omega)|_{x_3 = x_{3,R}} = \mathbf{I}\delta(\mathbf{x}_{\mathrm{H}} - \mathbf{x}_{\mathrm{H},R}), \tag{51}$$

($\mathbf{I}$ is the 3×3 identity matrix) and demand that $\mathbf{F}(\mathbf{x}, \mathbf{x}_R, \omega)$ is purely upgoing at $\partial \mathbb{D}_R$ and in the homogeneous isotropic upper half-space. Eq. (51) implies that, for the kth column of $\mathbf{F}$, the kth component of the particle velocity vector in that column focuses at $\mathbf{x}_R$ and the other two components are zero on $\partial \mathbb{D}_R$. Hence, the columns of $\mathbf{F}$ are mutually independent.

We discuss a representation for a wave field $v_k(\mathbf{x}, \omega)$, which may have sources in the upper half-space above $\partial \mathbb{D}_R$, but which obeys the source-free wave equation $\mathcal{L}_{ik} v_k = 0$ for $x_3 \geq x_{3,R}$. We store the components $v_k(\mathbf{x}, \omega)$ in a 3×1 vector $\mathbf{v}(\mathbf{x}, \omega)$ as follows:

$$\mathbf{v}(\mathbf{x}, \omega) = \begin{pmatrix} v_1 \\ v_2 \\ v_3 \end{pmatrix} (\mathbf{x}, \omega). \tag{52}$$

In the lower half-space we express $\mathbf{v}(\mathbf{x}, \omega)$ as a superposition of mutually independent wave fields that obey the same source-free wave equation as $\mathbf{v}(\mathbf{x}, \omega)$ for $x_3 \geq x_{3,R}$. For this purpose we choose the focusing functions $\mathbf{F}(\mathbf{x}, \mathbf{x}_R, \omega)$ and $\mathbf{F}^*(\mathbf{x}, \mathbf{x}_R, \omega)$, of which the columns are also mutually independent. Hence, analogous to eq. (10) we express $\mathbf{v}(\mathbf{x}, \omega)$ as

$$\mathbf{v}(\mathbf{x}, \omega) = \int_{\partial \mathbb{D}_R} \mathbf{F}(\mathbf{x}, \mathbf{x}_R, \omega) \mathbf{a}(\mathbf{x}_R, \omega) \mathrm{d}\mathbf{x}_R + \int_{\partial \mathbb{D}_R} \mathbf{F}^*(\mathbf{x}, \mathbf{x}_R, \omega) \mathbf{b}(\mathbf{x}_R, \omega) \mathrm{d}\mathbf{x}_R, \quad \text{for} \quad x_3 \geq x_{3,R}. \tag{53}$$

Here $\mathbf{a}(\mathbf{x}_R, \omega)$ and $\mathbf{b}(\mathbf{x}_R, \omega)$ are as yet undetermined 3×1 vectors. In Appendix B1, we formulate boundary conditions for the particle velocity and traction vectors at $\partial \mathbb{D}_R$, from which we solve $\mathbf{a}(\mathbf{x}_R, \omega)$ and $\mathbf{b}(\mathbf{x}_R, \omega)$. We thus obtain

$$\mathbf{v}(\mathbf{x}, \omega) = \int_{\partial \mathbb{D}_R} \mathbf{F}(\mathbf{x}, \mathbf{x}_R, \omega) \mathbf{v}^-(\mathbf{x}_R, \omega) \mathrm{d}\mathbf{x}_R + \int_{\partial \mathbb{D}_R} \mathbf{F}^*(\mathbf{x}, \mathbf{x}_R, \omega) \mathbf{v}^+(\mathbf{x}_R, \omega) \mathrm{d}\mathbf{x}_R, \quad \text{for} \quad x_3 \geq x_{3,R}, \tag{54}$$

where $\mathbf{v}^-(\mathbf{x}_R, \omega)$ and $\mathbf{v}^+(\mathbf{x}_R, \omega)$ represent the upgoing and downgoing parts, respectively, of $\mathbf{v}(\mathbf{x}_R, \omega)$ for $\mathbf{x}_R$ at $\partial \mathbb{D}_R$. These upgoing and downgoing fields are velocity-normalized, meaning that $\mathbf{v}^- + \mathbf{v}^+ = \mathbf{v}$ at and above $\partial \mathbb{D}_R$. Below $\partial \mathbb{D}_R$ we only consider the total (undecomposed) wave field $\mathbf{v}$.

The explanation of the right-hand side of eq. (54) in terms of Huygens' principle is similar to that of eq. (11). The main extension is that the matrix–vector products in eq. (54) accomplish a summation over the different components of the secondary sources at $\partial \mathbb{D}_R$ (corresponding to the foci of the different columns of the focusing function $\mathbf{F}$).

As for the acoustic representation of eq. (11), the underlying assumption in the derivation of eq. (54) is that evanescent waves can be neglected at $\partial \mathbb{D}_R$. Hence, it only holds for waves which have a horizontal slowness $\mathbf{s}$ which obeys

$$|\mathbf{s}| \leq 1/c_P, \quad \text{at } \partial \mathbb{D}_R. \tag{55}$$

Using similar arguments as given below eq. (12), it follows that eq. (54) accounts for evanescent waves inside the medium, as long as they are related to propagating waves at the surface, as formulated by eq. (55).

5 ELASTODYNAMIC GREEN'S FUNCTION REPRESENTATIONS

5.1 Representation for a modified elastodynamic Green's function

We introduce the elastodynamic Green's function $G_{k,n}(\mathbf{x}, \mathbf{x}_S, \omega)$ as a solution of eq. (48) for a unit point source of volume-force density at $\mathbf{x}_S$ in the x_n-direction, hence

$$\mathcal{L}_{ik} G_{k,n} = i\omega \delta_{in} \delta(\mathbf{x} - \mathbf{x}_S). \tag{56}$$

We demand that the time domain version of $G_{k,n}(\mathbf{x}, \mathbf{x}_S, \omega)$ is causal. Note that $G_{k,n}$ obeys source–receiver reciprocity, that is $G_{k,n}(\mathbf{x}, \mathbf{x}_S, \omega) = G_{n,k}(\mathbf{x}_S, \mathbf{x}, \omega)$. We introduce $\mathbf{G}(\mathbf{x}, \mathbf{x}_S, \omega)$ as a 3×3 matrix, according to

$$\mathbf{G}(\mathbf{x}, \mathbf{x}_S, \omega) = \begin{pmatrix} G_{1,1} & G_{1,2} & G_{1,3} \\ G_{2,1} & G_{2,2} & G_{2,3} \\ G_{3,1} & G_{3,2} & G_{3,3} \end{pmatrix} (\mathbf{x}, \mathbf{x}_S, \omega). \tag{57}$$

Each column is a particle velocity vector of which the components, for fixed $\mathbf{x}_S$ and variable $\mathbf{x}$, obey wave eq. (56). The different columns correspond to different directions of the force source at $\mathbf{x}_S$. This is different from the elastodynamic Green's function used by Wapenaar & Slob (2014), in which the different elements represent decomposed compressional and shear waves. In matrix form, source–receiver reciprocity implies $\mathbf{G}(\mathbf{x}, \mathbf{x}_S, \omega) = \{\mathbf{G}(\mathbf{x}_S, \mathbf{x}, \omega)\}^t$, where superscript t denotes transposition.

We choose $\mathbf{x}_S = (\mathbf{x}_{H,S}, x_{3,S})$ again in the upper half-space, at a vanishing distance ϵ above $\partial \mathbb{D}_R$, hence, $x_{3,S} = x_{3,R} - \epsilon$. In Appendix B2, we derive a modified version $\boldsymbol{\Gamma}(\mathbf{x}, \mathbf{x}_S, \omega)$ of $\mathbf{G}(\mathbf{x}, \mathbf{x}_S, \omega)$ (eq. B20), of which the downgoing part $\boldsymbol{\Gamma}^+(\mathbf{x}, \mathbf{x}_S, \omega)$ for $\mathbf{x}$ at $\partial \mathbb{D}_R$ (i.e. just below the source level) is equal to a spatial delta function. Hence

$$\boldsymbol{\Gamma}^+(\mathbf{x}, \mathbf{x}_S, \omega)|_{x_3=x_{3,R}} = \mathbf{I}\delta(\mathbf{x}_H - \mathbf{x}_{H,S}). \tag{58}$$

We define the reflection response $\mathbf{R}(\mathbf{x}_R, \mathbf{x}_S, \omega)$ of the medium below $\partial \mathbb{D}_R$ as the upgoing part of $\boldsymbol{\Gamma}(\mathbf{x}_R, \mathbf{x}_S, \omega)$, with $\mathbf{x}_R$ at $\partial \mathbb{D}_R$, hence

$$\mathbf{R}(\mathbf{x}_R, \mathbf{x}_S, \omega) = \boldsymbol{\Gamma}^-(\mathbf{x}_R, \mathbf{x}_S, \omega). \tag{59}$$

Substituting $\mathbf{v}(\mathbf{x}, \omega) = \boldsymbol{\Gamma}(\mathbf{x}, \mathbf{x}_S, \omega)$ and $\mathbf{v}^\pm(\mathbf{x}_R, \omega) = \boldsymbol{\Gamma}^\pm(\mathbf{x}_R, \mathbf{x}_S, \omega)$ into eq. (54), using eqs (58) and (59), gives

$$\boldsymbol{\Gamma}(\mathbf{x}, \mathbf{x}_S, \omega) = \int_{\partial \mathbb{D}_R} \mathbf{F}(\mathbf{x}, \mathbf{x}_R, \omega)\mathbf{R}(\mathbf{x}_R, \mathbf{x}_S, \omega)\mathrm{d}\mathbf{x}_R + \mathbf{F}^*(\mathbf{x}, \mathbf{x}_S, \omega), \quad \text{for} \quad x_3 \geq x_{3,R}. \tag{60}$$

This is a representation for the modified version $\boldsymbol{\Gamma}(\mathbf{x}, \mathbf{x}_S, \omega)$ of the elastodynamic Green's function. It has been derived without applying decomposition in the lower half-space. It only excludes the contribution from waves that are evanescent at $\partial \mathbb{D}_R$.

5.2 Representation for the elastodynamic Green's function

In Appendix B3 we show that eq. (60) can be reorganized into the following representation for the elastodynamic Green's function $\mathbf{G}(\mathbf{x}, \mathbf{x}_S, \omega)$

$$\mathbf{G}(\mathbf{x}, \mathbf{x}_S, \omega) = \int_{\partial \mathbb{D}_R} \mathbf{f}(\mathbf{x}, \mathbf{x}_R, \omega)\{\mathbf{R}(\mathbf{x}_S, \mathbf{x}_R, \omega)\}^t \mathrm{d}\mathbf{x}_R + \mathbf{f}^*(\mathbf{x}, \mathbf{x}_S, \omega), \quad \text{for} \quad x_3 \geq x_{3,R}. \tag{61}$$

Here $\mathbf{f}(\mathbf{x}, \mathbf{x}_R, \omega)$ is a modified version of the focusing function $\mathbf{F}(\mathbf{x}, \mathbf{x}_R, \omega)$ (eq. B25). This representation gives the full elastodynamic particle velocity field at any virtual receiver position $\mathbf{x}$ inside the medium. It is similar to earlier derived elastodynamic representations for the Marchenko method (da Costa Filho *et al.* 2014; Wapenaar & Slob 2014), but here it has been derived without applying decomposition at a truncation level inside the medium. As a consequence, eq. (61) gives the full wave field at any virtual receiver position $\mathbf{x}$ inside the medium, including multiply reflected, converted, refracted and evanescent waves. This representation only excludes the contribution from waves that are evanescent at $\partial \mathbb{D}_R$, see the condition formulated by eq. (55).

Applying elastodynamic representations like the one in eq. (61) to derive a Marchenko method is not trivial. The functions $\mathbf{G}(\mathbf{x}, \mathbf{x}_S, \omega)$ and $\mathbf{f}^*(\mathbf{x}, \mathbf{x}_S, \omega)$, transformed back to the time domain, partly overlap and hence they cannot be completely separated by a time window [similar as discussed by Wapenaar & Slob (2014) and Reinicke *et al.* (2020) for Green's functions and focusing functions consisting of decomposed compressional and shear waves]. A discussion of elastodynamic Marchenko methods is beyond the scope of this paper.

Similar as in the acoustic situation, the representation of eq. (61) is not a sufficient starting point for imaging. We need at least one other type of field at $\mathbf{x}$, next to $\mathbf{G}(\mathbf{x}, \mathbf{x}_S, \omega)$, which represents the particle velocity at $\mathbf{x}$ in response to force sources at $\mathbf{x}_S$. To this end, we introduce a Green's function $\mathbf{G}_j^\tau(\mathbf{x}, \mathbf{x}_S, \omega)$ which, for $j = 1, 2, 3$, stands for the three traction vectors at $\mathbf{x}$. From eq. (47) we derive that the traction vector $\boldsymbol{\tau}_j$ can be expressed in terms of the particle velocity as $\boldsymbol{\tau}_j = -\frac{1}{i\omega}\mathbf{C}_{jl}\partial_l\mathbf{v}$, with $(\boldsymbol{\tau}_j)_i = \tau_{ij}$ and $(\mathbf{C}_{jl})_{ik} = c_{ijkl}$. Similarly, we relate $\mathbf{G}_j^\tau$ to $\mathbf{G}$ via

$$\mathbf{G}_j^\tau(\mathbf{x}, \mathbf{x}_S, \omega) = -\frac{1}{i\omega}\mathbf{C}_{jl}(\mathbf{x})\partial_l\mathbf{G}(\mathbf{x}, \mathbf{x}_S, \omega). \tag{62}$$

Hence, when $\mathbf{G}(\mathbf{x}, \mathbf{x}_S, \omega)$ is available on a sufficiently dense grid, $\mathbf{G}_j^\tau(\mathbf{x}, \mathbf{x}_S, \omega)$ can be obtained via eq. (62). Alternatively, $\mathbf{G}_j^\tau(\mathbf{x}, \mathbf{x}_S, \omega)$ can be obtained from a modified version of the representation for $\mathbf{G}(\mathbf{x}, \mathbf{x}_S, \omega)$. Applying the operation $-\frac{1}{i\omega}\mathbf{C}_{jl}\partial_l$ to both sides of eq. (61) yields

$$\mathbf{G}_j^\tau(\mathbf{x}, \mathbf{x}_S, \omega) = \int_{\partial \mathbb{D}_R} \mathbf{h}_j(\mathbf{x}, \mathbf{x}_R, \omega)\{\mathbf{R}(\mathbf{x}_S, \mathbf{x}_R, \omega)\}^t \mathrm{d}\mathbf{x}_R - \mathbf{h}_j^*(\mathbf{x}, \mathbf{x}_S, \omega), \quad \text{for} \quad x_3 \geq x_{3,R}, \tag{63}$$

with

$$\mathbf{h}_j(\mathbf{x}, \mathbf{x}_R, \omega) = -\frac{1}{i\omega}\mathbf{C}_{jl}(\mathbf{x})\partial_l\mathbf{f}(\mathbf{x}, \mathbf{x}_R, \omega). \tag{64}$$

The Green's functions $\mathbf{G}(\mathbf{x}, \mathbf{x}_S, \omega)$ and $\mathbf{G}_j^\tau(\mathbf{x}, \mathbf{x}_S, \omega)$ together provide sufficient information for imaging.

5.3 Representation for the homogeneous elastodynamic Green's function

The representations in Sections 5.1 and 5.2 give the elastodynamic response to a source at $\mathbf{x}_S$, observed by a virtual receiver at $\mathbf{x}$ inside the medium. Similar as in Section 3.3, here we modify the representation of eq. (61), to create the response at the surface to a virtual source inside the medium. After that, we show how to obtain the response to this virtual source at a virtual receiver inside the medium.

We start by renaming the coordinate vectors in eq. (61) as follows: $\mathbf{x}_S \to \mathbf{x}_R$, $\mathbf{x}_R \to \mathbf{x}_S$, $\mathbf{x} \to \mathbf{x}_A$. This yields, in combination with transposing all terms and applying source–receiver reciprocity on the left-hand side of eq. (61),

$$\mathbf{G}(\mathbf{x}_R, \mathbf{x}_A, \omega) = \int_{\partial \mathbb{D}_R} \mathbf{R}(\mathbf{x}_R, \mathbf{x}_S, \omega) \mathbf{f}^t(\mathbf{x}_A, \mathbf{x}_S, \omega) \mathrm{d}\mathbf{x}_S + \mathbf{f}^\dagger(\mathbf{x}_A, \mathbf{x}_R, \omega), \quad \text{for} \quad x_{3,A} \geq x_{3,R}. \tag{65}$$

Here superscript † denotes transposition and complex conjugation. The integral in eq. (65) describes elastodynamic redatuming of the sources from all $\mathbf{x}_S$ at the surface to virtual-source position $\mathbf{x}_A$ in the subsurface.

Our next aim is to derive a representation for the response observed by a virtual receiver at $\mathbf{x}$ in the subsurface, given $\mathbf{G}(\mathbf{x}_R, \mathbf{x}_A, \omega)$. Similar as in Section 3.3, we define the homogeneous elastodynamic Green's function

$$\mathbf{G}_h(\mathbf{x}, \mathbf{x}_A, \omega) = \mathbf{G}(\mathbf{x}, \mathbf{x}_A, \omega) + \mathbf{G}^*(\mathbf{x}, \mathbf{x}_A, \omega). \tag{66}$$

The components of $\mathbf{G}(\mathbf{x}, \mathbf{x}_A, \omega)$ and $\mathbf{G}^*(\mathbf{x}, \mathbf{x}_A, \omega)$ obey eq. (56), with source terms $i\omega\delta_{in}\delta(\mathbf{x} - \mathbf{x}_A)$ and $-i\omega\delta_{in}\delta(\mathbf{x} - \mathbf{x}_A)$, respectively, on the right-hand sides. Hence, the components of $\mathbf{G}_h(\mathbf{x}, \mathbf{x}_A, \omega)$ obey this equation without a source on the right-hand side. Following a similar reasoning as in Section 3.3, we substitute

$$\mathbf{v}(\mathbf{x}, \omega) = \mathbf{G}_h(\mathbf{x}, \mathbf{x}_A, \omega), \tag{67}$$

$$\mathbf{v}^-(\mathbf{x}, \omega) = \mathbf{G}_h^-(\mathbf{x}, \mathbf{x}_A, \omega) = \mathbf{G}(\mathbf{x}, \mathbf{x}_A, \omega), \quad \text{for} \quad x_3 = x_{3,R}, \tag{68}$$

$$\mathbf{v}^+(\mathbf{x}, \omega) = \mathbf{G}_h^+(\mathbf{x}, \mathbf{x}_A, \omega) = \mathbf{G}^*(\mathbf{x}, \mathbf{x}_A, \omega), \quad \text{for} \quad x_3 = x_{3,R}, \tag{69}$$

into eq. (54). This gives

$$\mathbf{G}_h(\mathbf{x}, \mathbf{x}_A, \omega) = 2\Re \int_{\partial \mathbb{D}_R} \mathbf{F}(\mathbf{x}, \mathbf{x}_R, \omega) \mathbf{G}(\mathbf{x}_R, \mathbf{x}_A, \omega) \mathrm{d}\mathbf{x}_R, \quad \text{for} \quad x_3 \geq x_{3,R}. \tag{70}$$

This equation describes elastodynamic redatuming of the receivers from all $\mathbf{x}_R$ at the surface to virtual-receiver position $\mathbf{x}$ in the subsurface. It gives the homogeneous Green's function $\mathbf{G}_h(\mathbf{x}, \mathbf{x}_A, \omega)$, which is the response to the virtual source at $\mathbf{x}_A$, observed by a virtual receiver at $\mathbf{x}$, plus its complex conjugate. After transforming this to the time domain, $\mathbf{G}(\mathbf{x}, \mathbf{x}_A, t)$ can be extracted from $\mathbf{G}_h(\mathbf{x}, \mathbf{x}_A, t)$ by selecting its causal part.

An elastodynamic homogeneous Green's function representation similar to eq. (70) was also derived by Wapenaar *et al.* (2016b) and illustrated with numerical examples by Reinicke & Wapenaar (2019), but here the fields are not decomposed into downgoing and upgoing compressional and shear waves inside the medium. Hence, it also holds for evanescent waves inside the medium, as long as condition (55) is obeyed. Moreover, the derivation presented here is much simpler than in those references.

The source and receiver redatuming processes can be captured in one equation by substituting eq. (65) into (70). This gives

$$\mathbf{G}_h(\mathbf{x}, \mathbf{x}_A, \omega) = 2\Re \int_{\partial \mathbb{D}_R} \int_{\partial \mathbb{D}_R} \mathbf{F}(\mathbf{x}, \mathbf{x}_R, \omega) \mathbf{R}(\mathbf{x}_R, \mathbf{x}_S, \omega) \mathbf{f}^t(\mathbf{x}_A, \mathbf{x}_S, \omega) \mathrm{d}\mathbf{x}_S \mathrm{d}\mathbf{x}_R$$

$$+ 2\Re \int_{\partial \mathbb{D}_R} \mathbf{F}(\mathbf{x}, \mathbf{x}_R, \omega) \mathbf{f}^\dagger(\mathbf{x}_A, \mathbf{x}_R, \omega) \mathrm{d}\mathbf{x}_R, \quad \text{for} \quad \{x_3, x_{3,A}\} \geq x_{3,R}. \tag{71}$$

The double integral on the right-hand side resembles the process of classical elastodynamic source and receiver redatuming (Wapenaar & Berkhout 1989; Hokstad 2000), but with the primary focusing functions in those references replaced by full-field focusing functions. It also resembles elastodynamic source–receiver interferometry (Halliday *et al.* 2012), but with the double integration along a closed boundary in that paper replaced by the double integration over the open boundary $\partial \mathbb{D}_R$. Hence, via the theories of elastodynamic primary source–receiver redatuming (Wapenaar & Berkhout 1989; Hokstad 2000), closed-boundary source–receiver interferometry (Halliday *et al.* 2012) and open-boundary homogeneous Green's function retrieval using wave field decomposition (Wapenaar *et al.* 2016b), we have arrived at a representation for elastodynamic open-boundary homogeneous full-field Green's function retrieval (eq. 71), which accounts for internal multiples, converted, refracted and evanescent waves in the lower half-space.

6 CONCLUSIONS

We have derived acoustic and elastodynamic Green's function representations in terms of the reflection response at the surface and focusing functions. These representations have the same form as the representations that we derived earlier as the basis for Marchenko redatuming, imaging, monitoring and multiple elimination. However, unlike in our original derivations, we did not assume that the wave field inside the medium can be decomposed into downgoing and upgoing waves and we did not ignore evanescent waves inside the medium. We only neglected the contribution of waves that are evanescent at the acquisition boundary. We have demonstrated with numerical examples that the representations indeed account for evanescent waves inside the medium. The representations form a starting point for new research on Marchenko methods which circumvent the limitations caused by the assumptions underlying the traditional representations. In these new developments, care should be taken to account for the overlap in time of the Green's function and the time-reversed focusing function, particularly when dealing with refracted waves.

DATA AVAILABILITY

This study uses numerical data only. The codes used will be shared on reasonable request to the corresponding author.

REFERENCES

Behura, J., Wapenaar, K. & Snieder, R., 2014. Autofocus imaging: Image reconstruction based on inverse scattering theory, *Geophysics,* **79**(3), A19–A26.

Berkhout, A.J., 1982. *Seismic Migration. Imaging of Acoustic Energy by Wave Field Extrapolation. A. Theoretical Aspects,* Elsevier.

Berryhill, J.R., 1984. Wave-equation datuming before stack, *Geophysics,* **49**, 2064–2066.

Brackenhoff, J., Thorbecke, J. & Wapenaar, K., 2019. Monitoring of induced distributed double-couple sources using Marchenko-based virtual receivers, *Solid Earth,* **10**, 1301–1319.

Broggini, F. & Snieder, R., 2012. Connection of scattering principles: a visual and mathematical tour, *Eur. J. Phys.,* **33**, 593–613.

Broggini, F., Snieder, R. & Wapenaar, K., 2014. Data-driven wavefield focusing and imaging with multidimensional deconvolution: numerical examples for reflection data with internal multiples, *Geophysics,* **79**(3), WA107–WA115.

Burridge, R., 1980. The Gelfand-Levitan, the Marchenko, and the Gopinath-Sondhi integral equations of inverse scattering theory, regarded in the context of inverse impulse-response problems, *Wave Motion,* **2**, 305–323.

Corones, J.P., 1975. Bremmer series that correct parabolic approximations, *J. Math. Anal. Appl.,* **50**, 361–372.

Curtis, A. & Halliday, D., 2010. Source-receiver wavefield interferometry, *Phys. Rev. E,* **81**, 046601.

da Costa Filho, C.A., Ravasi, M., Curtis, A. & Meles, G.A., 2014. Elastodynamic Green's function retrieval through single-sided Marchenko inverse scattering, *Phys. Rev. E,* **90**, 063201.

Diekmann, L. & Vasconcelos, I., 2021. Focusing and Green's function retrieval in three-dimensional inverse scattering revisited: a single-sided Marchenko integral for the full wave field, *Phys. Rev. Research,* **3**, 013206.

Elison, P., Dukalski, M.S., de Vos, K., van Manen, D.J. & Robertsson, J.O.A., 2020. Data-driven control over short-period internal multiples in media with a horizontally layered overburden, *Geophys. J. Int.,* **221**, 769–787.

Fishman, L. & McCoy, J.J., 1984. Derivation and application of extended parabolic wave theories. I. The factorized Helmholtz equation, *J. Math. Phys.,* **25**(2), 285–296.

Halliday, D., Curtis, A. & Wapenaar, K., 2012. Generalized PP + PS = SS from seismic interferometry, *Geophys. J. Int.,* **189**, 1015–1024.

Hokstad, K., 2000. Multicomponent Kirchhoff migration, *Geophysics,* **65**(3), 861–873.

Holicki, M., Drijkoningen, G. & Wapenaar, K., 2019. Acoustic directional snapshot wavefield decomposition, *Geophys. Prosp.,* **67**, 32–51.

Jia, X., Guitton, A. & Snieder, R., 2018. A practical implementation of subsalt Marchenko imaging with a Gulf of Mexico data set, *Geophysics,* **83**(5), S409–S419.

Kennett, B.L.N., Kerry, N.J. & Woodhouse, J.H., 1978. Symmetries in the reflection and transmission of elastic waves, *Geophys. J. R. astr. Soc.,* **52**, 215–230.

Kiraz, M.S.R., Snieder, R. & Wapenaar, K., 2021. Focusing waves in an unknown medium without wavefield decomposition, *JASA Express Lett.,* **1**(5), 055602.

Liu, F., Zhang, G., Morton, S.A. & Leveille, J.P., 2011. An effective imaging condition for reverse-time migration using wavefield decomposition, *Geophysics,* **76**, S29–S39.

Lomas, A. & Curtis, A., 2019. An introduction to Marchenko methods for imaging, *Geophysics,* **84**(2), F35–F45.

Mildner, C., Broggini, F., de Vos, K. & Robertsson, J.O.A., 2019. Accurate source wavelet estimation using Marchenko focusing functions, *Geophysics,* **84**(6), Q73–Q88.

Oristaglio, M.L., 1989. An inverse scattering formula that uses all the data, *Inverse Probl.,* **5**, 1097–1105.

Pereira, R., Ramzy, M., Griscenco, P., Huard, B., Huang, H., Cypriano, L. & Khalil, A., 2019. Internal multiple attenuation for OBN data with overburden/target separation, in *Proceedings of the 89th Annual Meeting of the Society of Exploration Geophysicists,* pp. 4520–4524.

Porter, R.P., 1970. Diffraction-limited, scalar image formation with holograms of arbitrary shape, *J. Opt. Soc. Am.,* **60**, 1051–1059.

Ravasi, M. & Vasconcelos, I., 2021. An open-source framework for the implementation of large-scale integral operators with flexible, modern HPC solutions - enabling 3D Marchenko imaging by least squares inversion, *Geophysics,* **86**(early view), doi:10.1190/geo2020–0796.1.

Ravasi, M., Vasconcelos, I., Kritski, A., Curtis, A., da Costa Filho, C.A. & Meles, G.A., 2016. Target-oriented Marchenko imaging of a North Sea field, *Geophys. J. Int.,* **205**, 99–104.

Reinicke, C. & Wapenaar, K., 2019. Elastodynamic single-sided homogeneous Green's function representation: theory and numerical examples, *Wave Motion,* **89**, 245–264.

Reinicke, C., Dukalski, M. & Wapenaar, K., 2020. Comparison of monotonicity challenges encountered by the inverse scattering series and the Marchenko demultiple method for elastic waves, *Geophysics,* **85**(5), Q11–Q26.

Schoenberg, M. & Sen, P.N., 1983. Properties of a periodically stratified acoustic half-space and its relation to a Biot fluid, *J. acoust. Soc. Am.,* **73**, 61–67.

Singh, S. & Snieder, R., 2017. Source-receiver Marchenko redatuming: obtaining virtual receivers and virtual sources in the subsurface, *Geophysics,* **82**(3), Q13–Q21.

Slob, E., Wapenaar, K., Broggini, F. & Snieder, R., 2014. Seismic reflector imaging using internal multiples with Marchenko-type equations, *Geophysics,* **79**(2), S63–S76.

Staring, M. & Wapenaar, K., 2020. Three-dimensional Marchenko internal multiple attenuation on narrow azimuth streamer data of the Santos Basin, Brazil, *Geophys. Prosp.,* **68**, 1864–1877.

Staring, M., Pereira, R., Douma, H., van der Neut, J. & Wapenaar, K., 2018. Source-receiver Marchenko redatuming on field data using an adaptive double-focusing method, *Geophysics,* **83**(6), S579–S590.

Stoffa, P.L., 1989. *Tau-p - A Plane Wave Approach to the Analysis of Seismic Data,* Kluwer Academic Publishers.

Ursin, B., 1983. Review of elastic and electromagnetic wave propagation in horizontally layered media, *Geophysics,* **48**, 1063–1081.

Van der Neut, J., Johnson, J.L., van Wijk, K., Singh, S., Slob, E. & Wapenaar, K., 2017. A Marchenko equation for acoustic inverse source problems, *J. acoust. Soc. Am.,* **141**(6), 4332–4346.

Wapenaar, C.P.A. & Berkhout, A.J., 1989. *Elastic Wave Field Extrapolation,* Elsevier.

Wapenaar, K., 2020. The Marchenko method for evanescent waves, *Geophys. J. Int.,* **223**, 1412–1417.

Wapenaar, K. & Slob, E., 2014. On the Marchenko equation for multicomponent single-sided reflection data, *Geophys. J. Int.,* **199**, 1367–1371.

Wapenaar, K., Broggini, F., Slob, E. & Snieder, R., 2013. Three-dimensional single-sided Marchenko inverse scattering, data-driven focusing, Green's

function retrieval, and their mutual relations, *Phys. Rev. Lett.,* **110,** 084301.

Wapenaar, K., Thorbecke, J., van der Neut, J., Broggini, F., Slob, E. & Snieder, R., 2014. Marchenko imaging, *Geophysics,* **79**(3), WA39–WA57.

Wapenaar, K., Thorbecke, J. & van der Neut, J., 2016a. A single-sided homogeneous Green's function representation for holographic imaging, inverse scattering, time-reversal acoustics and interferometric Green's function retrieval, *Geophys. J. Int.,* **205,** 531–535.

Wapenaar, K., van der Neut, J. & Slob, E., 2016b. Unified double- and single-sided homogeneous Green's function representations, *Proc. R. Soc. A,* **472,** 20160162.

Yoon, K. & Marfurt, K.J., 2006. Reverse-time migration using the Poynting vector, *Explor. Geophys.,* **37,** 102–107.

Zhang, L. & Slob, E., 2020. A fast algorithm for multiple elimination and transmission compensation in primary reflections, *Geophys. J. Int.,* **221,** 371–377.

APPENDIX A: DERIVATION OF THE ACOUSTIC WAVE FIELD REPRESENTATION

A1 Derivation of the representation of eq. (11)

We derive expressions for the coefficients $a(\mathbf{x}_R, \omega)$ and $b(\mathbf{x}_R, \omega)$ in the acoustic wave field representation of eq. (10). We do this by formulating two boundary conditions at $\partial \mathbb{D}_R$. First, we consider the acoustic pressure $p(\mathbf{x}, \omega)$ at $\partial \mathbb{D}_R$. To this end, we evaluate eq. (10) for $\mathbf{x}$ at $\partial \mathbb{D}_R$. Using the focusing condition formulated in eq. (9) we thus obtain

$$
p(\mathbf{x}, \omega)|_{x_3 = x_{3,R}} = \int_{\partial \mathbb{D}_R} \delta(\mathbf{x}_H - \mathbf{x}_{H,R}) a(\mathbf{x}_R, \omega) \mathrm{d}\mathbf{x}_R + \int_{\partial \mathbb{D}_R} \delta(\mathbf{x}_H - \mathbf{x}_{H,R}) b(\mathbf{x}_R, \omega) \mathrm{d}\mathbf{x}_R,
$$
$$
= \{a(\mathbf{x}, \omega) + b(\mathbf{x}, \omega)\}_{x_3 = x_{3,R}}, \tag{A1}
$$

where we used $\mathbf{x}_R = (\mathbf{x}_{H,R}, x_{3,R})$. This is our first equation for the coefficients $a(\mathbf{x}_R, \omega)$ and $b(\mathbf{x}_R, \omega)$.

Next, we consider the vertical component of the particle velocity $v_3(\mathbf{x}, \omega)$ at $\partial \mathbb{D}_R$. From the Fourier transform of eq. (1), using $\rho_{jk} = \delta_{jk} \rho_0$ at $\partial \mathbb{D}_R$, we obtain $v_3(\mathbf{x}, \omega) = \frac{1}{i\omega\rho_0} \partial_3 p(\mathbf{x}, \omega)$ for $\mathbf{x}$ at $\partial \mathbb{D}_R$. Substituting eq. (10) gives

$$
v_3(\mathbf{x}, \omega) = \frac{1}{i\omega\rho_0} \int_{\partial \mathbb{D}_R} \partial_3 F(\mathbf{x}, \mathbf{x}_R, \omega) a(\mathbf{x}_R, \omega) \mathrm{d}\mathbf{x}_R + \frac{1}{i\omega\rho_0} \int_{\partial \mathbb{D}_R} \partial_3 F^*(\mathbf{x}, \mathbf{x}_R, \omega) b(\mathbf{x}_R, \omega) \mathrm{d}\mathbf{x}_R, \tag{A2}
$$

for $x_3 = x_{3,R}$. Applying the spatial Fourier transformation of eq. (40) to both sides of eq. (A2) gives

$$
\tilde{v}_3(\mathbf{s}, x_3, \omega) = \frac{1}{i\omega\rho_0} \int_{\partial \mathbb{D}_R} \partial_3 \tilde{F}(\mathbf{s}, x_3, \mathbf{x}_R, \omega) a(\mathbf{x}_R, \omega) \mathrm{d}\mathbf{x}_R + \frac{1}{i\omega\rho_0} \int_{\partial \mathbb{D}_R} \partial_3 \tilde{F}^*(-\mathbf{s}, x_3, \mathbf{x}_R, \omega) b(\mathbf{x}_R, \omega) \mathrm{d}\mathbf{x}_R, \tag{A3}
$$

for $x_3 = x_{3,R}$. At this depth level the focusing function is an upgoing field (see Fig. 1), hence it obeys the following one-way wave equation

$$
\partial_3 \tilde{F}(\mathbf{s}, x_3, \mathbf{x}_R, \omega)|_{x_3 = x_{3,R}} = -i\omega s_3 \tilde{F}(\mathbf{s}, x_{3,R}, \mathbf{x}_R, \omega), \tag{A4}
$$

with the vertical slowness s_3 defined as

$$
s_3 = \begin{cases} \sqrt{1/c_0^2 - \mathbf{s} \cdot \mathbf{s}}, & \text{for } \mathbf{s} \cdot \mathbf{s} \le 1/c_0^2 \\ i\sqrt{\mathbf{s} \cdot \mathbf{s} - 1/c_0^2}, & \text{for } \mathbf{s} \cdot \mathbf{s} > 1/c_0^2. \end{cases} \tag{A5}
$$

The two expressions in eq. (A5) represent the situation for propagating and evanescent waves, respectively. Applying the spatial Fourier transformation of eqs (40) to eq. (9) we further have

$$
\tilde{F}(\mathbf{s}, x_{3,R}, \mathbf{x}_R, \omega) = \exp\{-i\omega\mathbf{s} \cdot \mathbf{x}_{H,R}\}. \tag{A6}
$$

Substitution of eqs (A4) and (A6) into eq. (A3) for $x_3 = x_{3,R}$ gives

$$
\tilde{v}_3(\mathbf{s}, x_{3,R}, \omega) = -\frac{s_3}{\rho_0} \int_{\partial \mathbb{D}_R} \exp\{-i\omega\mathbf{s} \cdot \mathbf{x}_{H,R}\} a(\mathbf{x}_R, \omega) \mathrm{d}\mathbf{x}_R + \frac{s_3^*}{\rho_0} \int_{\partial \mathbb{D}_R} \exp\{-i\omega\mathbf{s} \cdot \mathbf{x}_{H,R}\} b(\mathbf{x}_R, \omega) \mathrm{d}\mathbf{x}_R
$$
$$
= -\frac{s_3}{\rho_0} \tilde{a}(\mathbf{s}, x_{3,R}, \omega) + \frac{s_3^*}{\rho_0} \tilde{b}(\mathbf{s}, x_{3,R}, \omega). \tag{A7}
$$

Combining the spatial Fourier transform of eq. (A1) with eq. (A7) gives

$$
\begin{pmatrix} \tilde{p} \\ \tilde{v}_3 \end{pmatrix}_{x_3 = x_{3,R}} = \begin{pmatrix} 1 & 1 \\ s_3^*/\rho_0 & -s_3/\rho_0 \end{pmatrix} \begin{pmatrix} \tilde{b} \\ \tilde{a} \end{pmatrix}_{x_3 = x_{3,R}}. \tag{A8}
$$

For $\mathbf{s} \cdot \mathbf{s} \le 1/c_0^2$ at $\partial \mathbb{D}_R$ we have $s_3^* = s_3$, see eq. (A5). Hence, for propagating waves, eq. (A8) is recognised as the well-known system that composes the total wave fields on the left-hand side from downgoing and upgoing fields on the right-hand side (Corones 1975; Ursin 1983; Fishman & McCoy 1984). Hence

$$
\tilde{b}(\mathbf{s}, x_{3,R}, \omega) = \tilde{p}^+(\mathbf{s}, x_{3,R}, \omega), \tag{A9}
$$

$$
\tilde{a}(\mathbf{s}, x_{3,R}, \omega) = \tilde{p}^-(\mathbf{s}, x_{3,R}, \omega), \tag{A10}
$$

for $\mathbf{s} \cdot \mathbf{s} \leq 1/c_0^2$ at $\partial\mathbb{D}_R$, where $\tilde{p}^+(\mathbf{s}, x_{3,R}, \omega)$ and $\tilde{p}^-(\mathbf{s}, x_{3,R}, \omega)$ are downgoing and upgoing fields, respectively, at $\partial\mathbb{D}_R$. Transforming these expressions back to the space domain, using

$$p^\pm(\mathbf{x}_R, \omega) = \frac{\omega^2}{4\pi^2} \int_{\mathbb{R}^2} \exp\{i\omega\mathbf{s} \cdot \mathbf{x}_{H,R}\} \tilde{p}^\pm(\mathbf{s}, x_{3,R}, \omega)d\mathbf{s} \tag{A11}$$

and similar expressions for $a(\mathbf{x}_R, \omega)$ and $b(\mathbf{x}_R, \omega)$, gives

$$b(\mathbf{x}_R, \omega) \approx p^+(\mathbf{x}_R, \omega), \tag{A12}$$

$$a(\mathbf{x}_R, \omega) \approx p^-(\mathbf{x}_R, \omega). \tag{A13}$$

The approximation signs signify that evanescent waves are neglected at $\partial\mathbb{D}_R$ [since eqs (A9) and (A10) hold for propagating waves only, whereas the inverse Fourier transformation involves an integration along all horizontal slownesses]. Substitution of eqs (A12) and (A13) into eq. (10) gives eq. (11).

A2 Analysis of the integral in eq. (23)

We analyze the integral in eq. (23). We show that we can transfer the operator $\partial_{3,R}$ from f to G^s, and that this is accompanied with a sign change. For a function of two space variables, $u(\mathbf{x}, \mathbf{x}_R, \omega)$, we define the spatial Fourier transform along the second space variable as

$$\tilde{u}(\mathbf{x}, \mathbf{s}, x_{3,R}, \omega) = \int_{\mathbb{R}^2} u(\mathbf{x}, \mathbf{x}_{H,R}, x_{3,R}, \omega) \exp\{i\omega\mathbf{s} \cdot \mathbf{x}_{H,R}\}d\mathbf{x}_{H,R}. \tag{A14}$$

Note the opposite sign in the exponential, compared with that in eq. (40). Using this Fourier transform and Parseval's theorem, we obtain for the integral in eq. (23)

$$\int_{\partial\mathbb{D}_R} \{\partial_{3,R} f(\mathbf{x}, \mathbf{x}_R, \omega)\} G^s(\mathbf{x}_S, \mathbf{x}_R, \omega)d\mathbf{x}_R = \frac{\omega^2}{4\pi^2} \int_{\mathbb{R}^2} \{\partial_{3,R} \tilde{f}(\mathbf{x}, -\mathbf{s}, x_{3,R}, \omega)\} \tilde{G}^s(\mathbf{x}_S, \mathbf{s}, x_{3,R}, \omega)d\mathbf{s}. \tag{A15}$$

Note that $\tilde{f}(\mathbf{x}, -\mathbf{s}, x_{3,R}, \omega)$ is differentiated with respect to the focal point depth $x_{3,R}$, hence, the one-way wave equation gets a sign opposite to that in eq. (A4), that is $\partial_{3,R} \tilde{f}(\mathbf{x}, -\mathbf{s}, x_{3,R}, \omega) = i\omega s_3 \tilde{f}(\mathbf{x}, -\mathbf{s}, x_{3,R}, \omega)$, with s_3 defined in eq. (A5). We transfer $i\omega s_3$ to the Green's function and use $i\omega s_3 \tilde{G}^s(\mathbf{x}_S, \mathbf{s}, x_{3,R}, \omega) = -\partial_{3,R} \tilde{G}^s(\mathbf{x}_S, \mathbf{s}, x_{3,R}, \omega)$ (which is a differentiation with respect to the source depth $x_{3,R}$). Making these substitutions in the right-hand side of eq. (A15) and applying Parseval's theorem again gives

$$-\frac{\omega^2}{4\pi^2} \int_{\mathbb{R}^2} \tilde{f}(\mathbf{x}, -\mathbf{s}, x_{3,R}, \omega)\partial_{3,R} \tilde{G}^s(\mathbf{x}_S, \mathbf{s}, x_{3,R}, \omega)d\mathbf{s} = -\int_{\partial\mathbb{D}_R} f(\mathbf{x}, \mathbf{x}_R, \omega)\partial_{3,R} G^s(\mathbf{x}_S, \mathbf{x}_R, \omega)d\mathbf{x}_R. \tag{A16}$$

Hence, we have transferred the operator $\partial_{3,R}$ under the integral in eq. (23) from f to G^s, which involves a sign change.

APPENDIX B: DERIVATION OF THE ELASTODYNAMIC WAVE FIELD REPRESENTATION

B1 Derivation of the representation of eq. (54)

We derive expressions for the coefficients $\mathbf{a}(\mathbf{x}_R, \omega)$ and $\mathbf{b}(\mathbf{x}_R, \omega)$ in the elastodynamic wave field representation of eq. (53). We do this by formulating two boundary conditions at $\partial\mathbb{D}_R$. First, we consider the particle velocity vector $\mathbf{v}(\mathbf{x}, \omega)$ at $\partial\mathbb{D}_R$. To this end, we evaluate eq. (53) for $\mathbf{x}$ at $\partial\mathbb{D}_R$. Using the focusing condition formulated in eq. (51) we thus obtain

$$\begin{aligned} \mathbf{v}(\mathbf{x}, \omega)|_{x_3=x_{3,R}} &= \int_{\partial\mathbb{D}_R} \delta(\mathbf{x}_H - \mathbf{x}_{H,R})\mathbf{a}(\mathbf{x}_R, \omega)d\mathbf{x}_R + \int_{\partial\mathbb{D}_R} \delta(\mathbf{x}_H - \mathbf{x}_{H,R})\mathbf{b}(\mathbf{x}_R, \omega)d\mathbf{x}_R, \\ &= \{\mathbf{a}(\mathbf{x}, \omega) + \mathbf{b}(\mathbf{x}, \omega)\}_{x_3=x_{3,R}}. \end{aligned} \tag{B1}$$

For the second boundary condition we analyze the traction vector $\boldsymbol{\tau}_3(\mathbf{x}, \omega)$ at $\partial\mathbb{D}_R$. First we establish a relation between $\boldsymbol{\tau}_3(\mathbf{x}, \omega)$ and $\mathbf{v}(\mathbf{x}, \omega)$ in the homogeneous isotropic upper half-space, including $\partial\mathbb{D}_R$. Using eq. (40), we transform $\mathbf{v}(\mathbf{x}, \omega)$ and $\boldsymbol{\tau}_3(\mathbf{x}, \omega)$ for $x_3 \leq x_{3,R}$ to $\tilde{\mathbf{v}}(\mathbf{s}, x_3, \omega)$ and $\tilde{\boldsymbol{\tau}}_3(\mathbf{s}, x_3, \omega)$, respectively. These fields can be related to vectors $\tilde{\mathbf{p}}^+$ and $\tilde{\mathbf{p}}^-$ containing downgoing and upgoing compressional and shear wave fields, according to

$$\begin{pmatrix} \tilde{\mathbf{v}} \\ -\tilde{\boldsymbol{\tau}}_3 \end{pmatrix} = \begin{pmatrix} \tilde{\mathbf{L}}_1^+ & \tilde{\mathbf{L}}_1^- \\ \tilde{\mathbf{L}}_2^+ & \tilde{\mathbf{L}}_2^- \end{pmatrix} \begin{pmatrix} \tilde{\mathbf{p}}^+ \\ \tilde{\mathbf{p}}^- \end{pmatrix}, \quad \text{for} \quad x_3 \leq x_{3,R}, \tag{B2}$$

(Kennett *et al.* 1978; Ursin 1983; Wapenaar & Berkhout 1989). Next, we define the downgoing and upgoing parts of $\tilde{\mathbf{v}}$ as $\tilde{\mathbf{v}}^\pm = \tilde{\mathbf{L}}_1^\pm \tilde{\mathbf{p}}^\pm$ and rewrite eq. (B2) as

$$\begin{pmatrix} \tilde{\mathbf{v}} \\ -\tilde{\boldsymbol{\tau}}_3 \end{pmatrix} = \begin{pmatrix} \mathbf{I} & \mathbf{I} \\ \tilde{\mathbf{D}}^+ & \tilde{\mathbf{D}}^- \end{pmatrix} \begin{pmatrix} \tilde{\mathbf{v}}^+ \\ \tilde{\mathbf{v}}^- \end{pmatrix}, \quad \text{for} \quad x_3 \leq x_{3,R}, \tag{B3}$$

with $\tilde{\mathbf{D}}^\pm = \tilde{\mathbf{L}}_2^\pm (\tilde{\mathbf{L}}_1^\pm)^{-1}$. The matrices $\tilde{\mathbf{L}}_1^\pm$ and $\tilde{\mathbf{L}}_2^\pm$ in eq. (B2) are not uniquely defined. They depend on the chosen normalization of the fields contained in $\tilde{\mathbf{p}}^+$ and $\tilde{\mathbf{p}}^-$. However, independent of the normalization, the matrix $\tilde{\mathbf{D}}^\pm$ in eq. (B3) is uniquely defined. It is given by

$$\tilde{\mathbf{D}}^\pm(\mathbf{s}) = \frac{\rho_0 c_S^2}{s_3^P s_3^S + \mathbf{s} \cdot \mathbf{s}} \begin{pmatrix} \pm((c_S^{-2} - s_2^2)s_3^P + s_2^2 s_3^S) & \pm s_1 s_2 (s_3^P - s_3^S) & -s_1(c_S^{-2} - 2(s_3^P s_3^S + \mathbf{s} \cdot \mathbf{s})) \\ \pm s_1 s_2 (s_3^P - s_3^S) & \pm((c_S^{-2} - s_1^2)s_3^P + s_1^2 s_3^S) & -s_2(c_S^{-2} - 2(s_3^P s_3^S + \mathbf{s} \cdot \mathbf{s})) \\ s_1(c_S^{-2} - 2(s_3^P s_3^S + \mathbf{s} \cdot \mathbf{s})) & s_2(c_S^{-2} - 2(s_3^P s_3^S + \mathbf{s} \cdot \mathbf{s})) & \pm s_3^S c_S^{-2} \end{pmatrix} \tag{B4}$$

with the vertical slownesses s_3^P and s_3^S for P and S waves, respectively, defined as

$$s_3^{P,S} = \begin{cases} \sqrt{1/c_{P,S}^2 - \mathbf{s} \cdot \mathbf{s}}, & \text{for } \mathbf{s} \cdot \mathbf{s} \leq 1/c_{P,S}^2 \\ i\sqrt{\mathbf{s} \cdot \mathbf{s} - 1/c_{P,S}^2}, & \text{for } \mathbf{s} \cdot \mathbf{s} > 1/c_{P,S}^2, \end{cases} \tag{B5}$$

where c_P and c_S are the P- and S-wave velocities, respectively, of the upper half-space $x_3 \leq x_{3,R}$. Applying the transform of eq. (40) to eq. (53) we obtain for $\mathbf{x}$ at $\partial \mathbb{D}_R$

$$\tilde{\mathbf{v}}(\mathbf{s}, x_{3,R}, \omega) = \int_{\partial \mathbb{D}_R} \tilde{\mathbf{F}}(\mathbf{s}, x_{3,R}, \mathbf{x}_R, \omega) \mathbf{a}(\mathbf{x}_R, \omega) d\mathbf{x}_R + \int_{\partial \mathbb{D}_R} \tilde{\mathbf{F}}^*(-\mathbf{s}, x_{3,R}, \mathbf{x}_R, \omega) \mathbf{b}(\mathbf{x}_R, \omega) d\mathbf{x}_R. \tag{B6}$$

Since $\tilde{\mathbf{F}}(\mathbf{s}, x_{3,R}, \mathbf{x}_R, \omega)$ is upgoing, the first term on the right-hand side is the upgoing velocity field $\tilde{\mathbf{v}}^-(\mathbf{s}, x_{3,R}, \omega)$ and the second term is, for propagating waves (i.e., for $\mathbf{s} \cdot \mathbf{s} \leq 1/c_P^2$), the downgoing velocity field $\tilde{\mathbf{v}}^+(\mathbf{s}, x_{3,R}, \omega)$. Hence, using eq. (B3) we obtain for the transformed traction vector

$$-\tilde{\boldsymbol{\tau}}_3(\mathbf{s}, x_{3,R}, \omega) = \tilde{\mathbf{D}}^-(\mathbf{s}) \int_{\partial \mathbb{D}_R} \tilde{\mathbf{F}}(\mathbf{s}, x_{3,R}, \mathbf{x}_R, \omega) \mathbf{a}(\mathbf{x}_R, \omega) d\mathbf{x}_R + \tilde{\mathbf{D}}^+(\mathbf{s}) \int_{\partial \mathbb{D}_R} \tilde{\mathbf{F}}^*(-\mathbf{s}, x_{3,R}, \mathbf{x}_R, \omega) \mathbf{b}(\mathbf{x}_R, \omega) d\mathbf{x}_R, \tag{B7}$$

for $\mathbf{s} \cdot \mathbf{s} \leq 1/c_P^2$ at $\partial \mathbb{D}_R$. Applying the transform of eq. (40) to the focusing condition of eq. (51) gives

$$\tilde{\mathbf{F}}(\mathbf{s}, x_{3,R}, \mathbf{x}_R, \omega) = \mathbf{I} \exp\{-i\omega \mathbf{s} \cdot \mathbf{x}_{H,R}\}. \tag{B8}$$

Substituting this into eq. (B7) we obtain

$$-\tilde{\boldsymbol{\tau}}_3(\mathbf{s}, x_{3,R}, \omega) = \tilde{\mathbf{D}}^-(\mathbf{s})\tilde{\mathbf{a}}(\mathbf{s}, x_{3,R}, \omega) + \tilde{\mathbf{D}}^+(\mathbf{s})\tilde{\mathbf{b}}(\mathbf{s}, x_{3,R}, \omega), \tag{B9}$$

for $\mathbf{s} \cdot \mathbf{s} \leq 1/c_P^2$ at $\partial \mathbb{D}_R$. Combining this equation with the Fourier transform of eq. (B1) yields

$$\begin{pmatrix} \tilde{\mathbf{v}} \\ -\tilde{\boldsymbol{\tau}}_3 \end{pmatrix}_{x_3 = x_{3,R}} = \begin{pmatrix} \mathbf{I} & \mathbf{I} \\ \tilde{\mathbf{D}}^+ & \tilde{\mathbf{D}}^- \end{pmatrix} \begin{pmatrix} \tilde{\mathbf{b}} \\ \tilde{\mathbf{a}} \end{pmatrix}_{x_3 = x_{3,R}}, \tag{B10}$$

for $\mathbf{s} \cdot \mathbf{s} \leq 1/c_P^2$ at $\partial \mathbb{D}_R$. Comparing this with eq. (B3) we conclude

$$\tilde{\mathbf{b}}(\mathbf{s}, x_{3,R}, \omega) = \tilde{\mathbf{v}}^+(\mathbf{s}, x_{3,R}, \omega), \tag{B11}$$

$$\tilde{\mathbf{a}}(\mathbf{s}, x_{3,R}, \omega) = \tilde{\mathbf{v}}^-(\mathbf{s}, x_{3,R}, \omega), \tag{B12}$$

for $\mathbf{s} \cdot \mathbf{s} \leq 1/c_P^2$ at $\partial \mathbb{D}_R$. Transforming these expressions back to the space domain gives

$$\mathbf{b}(\mathbf{x}_R, \omega) \approx \mathbf{v}^+(\mathbf{x}_R, \omega), \tag{B13}$$

$$\mathbf{a}(\mathbf{x}_R, \omega) \approx \mathbf{v}^-(\mathbf{x}_R, \omega). \tag{B14}$$

The approximation signs signify that evanescent waves are neglected at $\partial \mathbb{D}_R$. Substitution of eqs (B13) and (B14) into eq. (53) gives eq. (54).

B2 Derivation of the modified elastodynamic Green's function

We derive a modified elastodynamic Green's function $\boldsymbol{\Gamma}(\mathbf{x}, \mathbf{x}_S, \omega)$ (with $x_{3,S} = x_{3,R} - \epsilon$), such that for $\mathbf{x}$ at $\partial \mathbb{D}_R$, that is just below the source level, the downgoing part of $\boldsymbol{\Gamma}(\mathbf{x}, \mathbf{x}_S, \omega)$ obeys eq. (58), that is

$$\lim_{x_3 \downarrow x_{3,S}} \boldsymbol{\Gamma}^+(\mathbf{x}, \mathbf{x}_S, \omega) = \mathbf{I}\delta(\mathbf{x}_H - \mathbf{x}_{H,S}). \tag{B15}$$

To this end we first investigate the properties of the downgoing part of $\mathbf{G}(\mathbf{x}, \mathbf{x}_S, \omega)$ defined in eqs (56) and (57), just below the source level. Consider the inverse of eq. (B3)

$$\begin{pmatrix} \tilde{\mathbf{v}}^+ \\ \tilde{\mathbf{v}}^- \end{pmatrix} = \begin{pmatrix} -\tilde{\boldsymbol{\Delta}}^{-1}\tilde{\mathbf{D}}^- & \tilde{\boldsymbol{\Delta}}^{-1} \\ \tilde{\boldsymbol{\Delta}}^{-1}\tilde{\mathbf{D}}^+ & -\tilde{\boldsymbol{\Delta}}^{-1} \end{pmatrix} \begin{pmatrix} \tilde{\mathbf{v}} \\ -\tilde{\boldsymbol{\tau}}_3 \end{pmatrix}, \quad \text{for} \quad x_3 \leq x_{3,R}, \tag{B16}$$

with

$$\tilde{\boldsymbol{\Delta}} = \tilde{\mathbf{D}}^+ - \tilde{\mathbf{D}}^-. \tag{B17}$$

The upper-right matrix in eq. (B16), $\tilde{\boldsymbol{\Delta}}^{-1}$, gives the relation between $-\tilde{\boldsymbol{\tau}}_3$ and the downgoing velocity vector $\tilde{\mathbf{v}}^+$. The same matrix transforms a unit force source in a homogeneous half-space into the downgoing part of the Green's function just below this source, hence

$$\lim_{x_3 \downarrow x_{3,S}} \tilde{\mathbf{G}}^+(\mathbf{s}, x_3, \mathbf{0}, x_{3,S}, \omega) = \tilde{\boldsymbol{\Delta}}^{-1}(\mathbf{s})$$

$$= \frac{1}{2\rho_0} \begin{pmatrix} \frac{s_1^2}{s_3^P} + \left(\frac{1}{c_S^2} - s_1^2\right)\frac{1}{s_3^S} & \left(\frac{1}{s_3^P} - \frac{1}{s_3^S}\right)s_1 s_2 & 0 \\ \left(\frac{1}{s_3^P} - \frac{1}{s_3^S}\right)s_1 s_2 & \frac{s_2^2}{s_3^P} + \left(\frac{1}{c_S^2} - s_2^2\right)\frac{1}{s_3^S} & 0 \\ 0 & 0 & s_3^P + \frac{\mathbf{s} \cdot \mathbf{s}}{s_3^S} \end{pmatrix}. \tag{B18}$$

In eq. (B18) the source is located at $(\mathbf{0}, x_{3,S})$. Next, we consider $\mathbf{G}(\mathbf{x}, \mathbf{x}_S, \omega)$ for a laterally shifted source position $(\mathbf{x}_{H,S}, x_{3,S})$. Applying a spatial Fourier transform along the horizontal source coordinate $\mathbf{x}_{H,S}$, using eq. (A14) with $\mathbf{x}_{H,R}$ replaced by $\mathbf{x}_{H,S}$, yields $\tilde{\mathbf{G}}(\mathbf{x}, \mathbf{s}, x_{3,S}, \omega)$. For the downgoing part just below the source we obtain a phase-shifted version of the Green's function of eq. (B18), according to

$$\lim_{x_3 \downarrow x_{3,S}} \tilde{\mathbf{G}}^+(\mathbf{x}, \mathbf{s}, x_{3,S}, \omega) = \tilde{\boldsymbol{\Delta}}^{-1}(\mathbf{s}) \exp\{i\omega\mathbf{s} \cdot \mathbf{x}_H\}. \tag{B19}$$

Comparing this with the desired condition of eq. (B15) suggests to define the modified Green's function (for arbitrary $\mathbf{x}$) as

$$\tilde{\boldsymbol{\Gamma}}(\mathbf{x}, \mathbf{s}, x_{3,S}, \omega) = \tilde{\mathbf{G}}(\mathbf{x}, \mathbf{s}, x_{3,S}, \omega)\tilde{\boldsymbol{\Delta}}(\mathbf{s}), \tag{B20}$$

such that

$$\lim_{x_3 \downarrow x_{3,S}} \tilde{\boldsymbol{\Gamma}}^+(\mathbf{x}, \mathbf{s}, x_{3,S}, \omega) = \mathbf{I} \exp\{i\omega\mathbf{s} \cdot \mathbf{x}_H\}. \tag{B21}$$

The inverse Fourier transform from $\mathbf{s}$ to $\mathbf{x}_{H,S}$ gives indeed eq. (B15).

We define the reflection response $\tilde{\mathbf{R}}(\mathbf{x}_R, \mathbf{s}, x_{3,S}, \omega)$ of the medium below $\partial\mathbb{D}_R$ as the upgoing part of the modified Green's function $\tilde{\boldsymbol{\Gamma}}(\mathbf{x}_R, \mathbf{s}, x_{3,S}, \omega)$, with $\mathbf{x}_R$ at $\partial\mathbb{D}_R$, hence

$$\tilde{\mathbf{R}}(\mathbf{x}_R, \mathbf{s}, x_{3,S}, \omega) = \tilde{\boldsymbol{\Gamma}}^-(\mathbf{x}_R, \mathbf{s}, x_{3,S}, \omega), \tag{B22}$$

or, using eq. (B20),

$$\tilde{\mathbf{R}}(\mathbf{x}_R, \mathbf{s}, x_{3,S}, \omega) = \tilde{\mathbf{G}}^-(\mathbf{x}_R, \mathbf{s}, x_{3,S}, \omega)\tilde{\boldsymbol{\Delta}}(\mathbf{s})$$

$$= \tilde{\mathbf{G}}^s(\mathbf{x}_R, \mathbf{s}, x_{3,S}, \omega)\tilde{\boldsymbol{\Delta}}(\mathbf{s}), \tag{B23}$$

where superscript s stands for scattered. The inverse Fourier transform of eq. (B22) from $\mathbf{s}$ to $\mathbf{x}_{H,S}$ yields eq. (59).

B3 Derivation of the representation of eq. (61)

To obtain a representation for $\mathbf{G}(\mathbf{x}, \mathbf{x}_S, \omega)$ we start by transforming all terms in eq. (60) along $\mathbf{x}_{H,S}$, using eq. (A14), with $\mathbf{x}_{H,R}$ replaced by $\mathbf{x}_{H,S}$, hence

$$\tilde{\boldsymbol{\Gamma}}(\mathbf{x}, \mathbf{s}, x_{3,S}, \omega) = \int_{\partial\mathbb{D}_R} \mathbf{F}(\mathbf{x}, \mathbf{x}_R, \omega)\tilde{\mathbf{R}}(\mathbf{x}_R, \mathbf{s}, x_{3,S}, \omega)d\mathbf{x}_R + \tilde{\mathbf{F}}^*(\mathbf{x}, -\mathbf{s}, x_{3,S}, \omega), \quad \text{for} \quad x_3 \geq x_{3,R}. \tag{B24}$$

We introduce a modified focusing function $\tilde{\mathbf{f}}(\mathbf{x}, \mathbf{s}, x_{3,S}, \omega)$ via

$$\tilde{\mathbf{F}}(\mathbf{x}, \mathbf{s}, x_{3,S}, \omega) = \tilde{\mathbf{f}}(\mathbf{x}, \mathbf{s}, x_{3,S}, \omega)\tilde{\boldsymbol{\Delta}}(\mathbf{s}). \tag{B25}$$

According to eq. (B18) we have for propagating waves (i.e. for $\mathbf{s} \cdot \mathbf{s} \leq 1/c_P^2$)

$$\tilde{\boldsymbol{\Delta}}(\mathbf{s}) = \tilde{\boldsymbol{\Delta}}(-\mathbf{s}) = \tilde{\boldsymbol{\Delta}}^*(\mathbf{s}) = \tilde{\boldsymbol{\Delta}}^t(\mathbf{s}). \tag{B26}$$

Hence, for $\tilde{\mathbf{F}}^*(\mathbf{x}, -\mathbf{s}, x_{3,S}, \omega)$ we obtain

$$\tilde{\mathbf{F}}^*(\mathbf{x}, -\mathbf{s}, x_{3,S}, \omega) = \tilde{\mathbf{f}}^*(\mathbf{x}, -\mathbf{s}, x_{3,S}, \omega)\tilde{\boldsymbol{\Delta}}(\mathbf{s}). \tag{B27}$$

Multiplying all terms in eq. (B24) from the right by $\tilde{\boldsymbol{\Delta}}^{-1}(\mathbf{s})$, using eqs (B20), (B23) and (B27), and transforming the resulting expression back from $\mathbf{s}$ to $\mathbf{x}_{H,S}$ gives

$$\mathbf{G}(\mathbf{x}, \mathbf{x}_S, \omega) = \int_{\partial\mathbb{D}_R} \mathbf{F}(\mathbf{x}, \mathbf{x}_R, \omega)\mathbf{G}^s(\mathbf{x}_R, \mathbf{x}_S, \omega)d\mathbf{x}_R + \mathbf{f}^*(\mathbf{x}, \mathbf{x}_S, \omega), \quad \text{for} \quad x_3 \geq x_{3,R}. \tag{B28}$$

We modify the integral step by step. First we use source–receiver reciprocity for the scattered Green's function $\mathbf{G}^s(\mathbf{x}_R, \mathbf{x}_S, \omega)$ and we apply Parseval's theorem. We thus obtain for the integral in eq. (B28)

$$\frac{\omega^2}{4\pi^2} \int_{\mathbb{R}^2} \tilde{\mathbf{F}}(\mathbf{x}, -\mathbf{s}, x_{3,R}, \omega)\{\tilde{\mathbf{G}}^s(\mathbf{x}_S, \mathbf{s}, x_{3,R}, \omega)\}^t d\mathbf{s}. \tag{B29}$$

Substituting eq. (B25), using eq. (B26), gives

$$\frac{\omega^2}{4\pi^2} \int_{\mathbb{R}^2} \tilde{\mathbf{f}}(\mathbf{x}, -\mathbf{s}, x_{3,R}, \omega) \{\tilde{\mathbf{G}}^s(\mathbf{x}_S, \mathbf{s}, x_{3,R}, \omega) \tilde{\boldsymbol{\Delta}}(\mathbf{s})\}^t \, d\mathbf{s}. \tag{B30}$$

Using eq. (B23) this gives

$$\frac{\omega^2}{4\pi^2} \int_{\mathbb{R}^2} \tilde{\mathbf{f}}(\mathbf{x}, -\mathbf{s}, x_{3,R}, \omega) \{\tilde{\mathbf{R}}(\mathbf{x}_S, \mathbf{s}, x_{3,R}, \omega)\}^t \, d\mathbf{s}. \tag{B31}$$

Applying Parseval's theorem again and inserting the resulting integral in eq. (B28) yields eq. (61). It has been derived without applying decomposition in the lower half-space, but it excludes the contribution from waves that are evanescent at $\partial \mathbb{D}_R$.